AGU PUBLICATIONS

Geochemistry, Geophysics, Geosystems

RESEARCH ARTICLE
10.1002/2015GC005969

Key Points:
- W to E Cretaceous scarp migration across plateau from AHe data and kimberlite constraints
- Lithospheric modification and erosion histories are different on-craton and off-craton
- Lithospheric structure is important for the surface expression of mantle dynamics

Supporting Information:
- Supporting Information S1
- Table S1

Correspondence to:
J. Stanley,
jessica.stanley@colorado.edu

Citation:
Stanley, J. R., R. M. Flowers, and D. R. Bell (2015), Erosion patterns and mantle sources of topographic change across the southern African Plateau derived from the shallow and deep records of kimberlites, *Geochem. Geophys. Geosyst.*, *16*, doi:10.1002/2015GC005969.

Received 17 JUN 2015
Accepted 3 SEP 2015
Accepted article online 7 SEP 2015

Erosion patterns and mantle sources of topographic change across the southern African Plateau derived from the shallow and deep records of kimberlites

Jessica R. Stanley[1], Rebecca M. Flowers[1], and David R. Bell[2]

[1]Department of Geological Sciences, University of Colorado, Boulder, Colorado, USA, [2]AEON-ESSRI, Nelson Mandela Metropolitan University, Port Elizabeth, South Africa

Abstract Flow in the sublithospheric mantle is increasingly invoked as a mechanism to explain both modern and past surface topography, but the importance of this phenomenon and its influence at different localities are debated. Southern Africa is an elevated continental shield proposed to represent dynamically supported topography. However, this region is also characterized by a complex lithospheric architecture variably affected by Cretaceous heating, thinning, and metasomatic alteration. We used apatite (U-Th)/He thermochronometry on 15 Cretaceous kimberlites from an ~600 km long transect across the Kaapvaal Craton, combined with information from xenoliths in these pipes, to determine the plateau interior erosion history. The goal was to determine the relationships with lithospheric modification patterns and thereby better isolate the sublithospheric contribution to elevation. The results document a wave of erosion from west to east across the craton from ~120 to <60 Ma, initially focused along paleorivers and then retreating as a scarp across the landscape. This spatially variable erosion event was associated with limited modification of the Archean cratonic lithospheric mantle as recorded by mantle xenoliths and xenocrysts, implying that dynamic buoyancy sources may be required to explain the elevations. In contrast, off-craton to the southwest, a more pronounced regional erosion phase at ~110–90 Ma was coincident with significant modification of the Proterozoic lithospheric mantle. This relationship suggests that lithospheric processes were more important contributors to erosion and topographic change off-craton than on-craton. Together, these results suggest that lithospheric architecture can have an important control on the surface expression of mantle dynamics.

1. Introduction

Most of the Earth's topography is caused by variability in the thickness and density of the crust and mantle lithosphere. However, dynamic topography, defined here as topography caused by viscous forces induced by the convecting mantle at the base of the lithosphere, has also been interpreted as significant in a diversity of settings and scales [e.g., *Lithgow-Bertelloni and Silver*, 1998; *Liu and Gurnis*, 2008; *Faccenna and Becker*, 2010; *Moucha and Forte*, 2011; *Flament et al*., 2013; *Rowley et al*., 2013]. Most predictions of dynamic topography rely on converting seismic velocities to density variations and either calculating residual topography by removing the isostatic contribution of the lithosphere, or by predicting the induced topography based in mantle flow. The magnitudes of both the calculated residual topography and the predicted dynamic topography vary widely even within the same geographic region [e.g., *Flament et al*., 2013] but are generally thought to be less than 1000 m [*Braun*, 2010].

The variability in model predictions of dynamic topography highlights the need to test them with geologic observations, providing a basis from which to further improve the models. Two challenges in this effort are discerning topographic change in the geologic record, and distinguishing deeply sourced topography from causes of topographic change within the mantle lithosphere and crust. Directly measuring uplift or subsidence from the geologic record is difficult, but the erosional and depositional responses to these phenomena can be detected using thermochronometry and the stratigraphic record. In several cases, regional stratigraphic [e.g., *Mitrovica et al*., 1989; *Liu et al*., 2008; *Spasojevic et al*., 2009] or thermal [e.g., *Flowers et al*., 2012; *Zhang et al*., 2012; *Ault et al*., 2013] histories have been linked to probable dynamic causes.

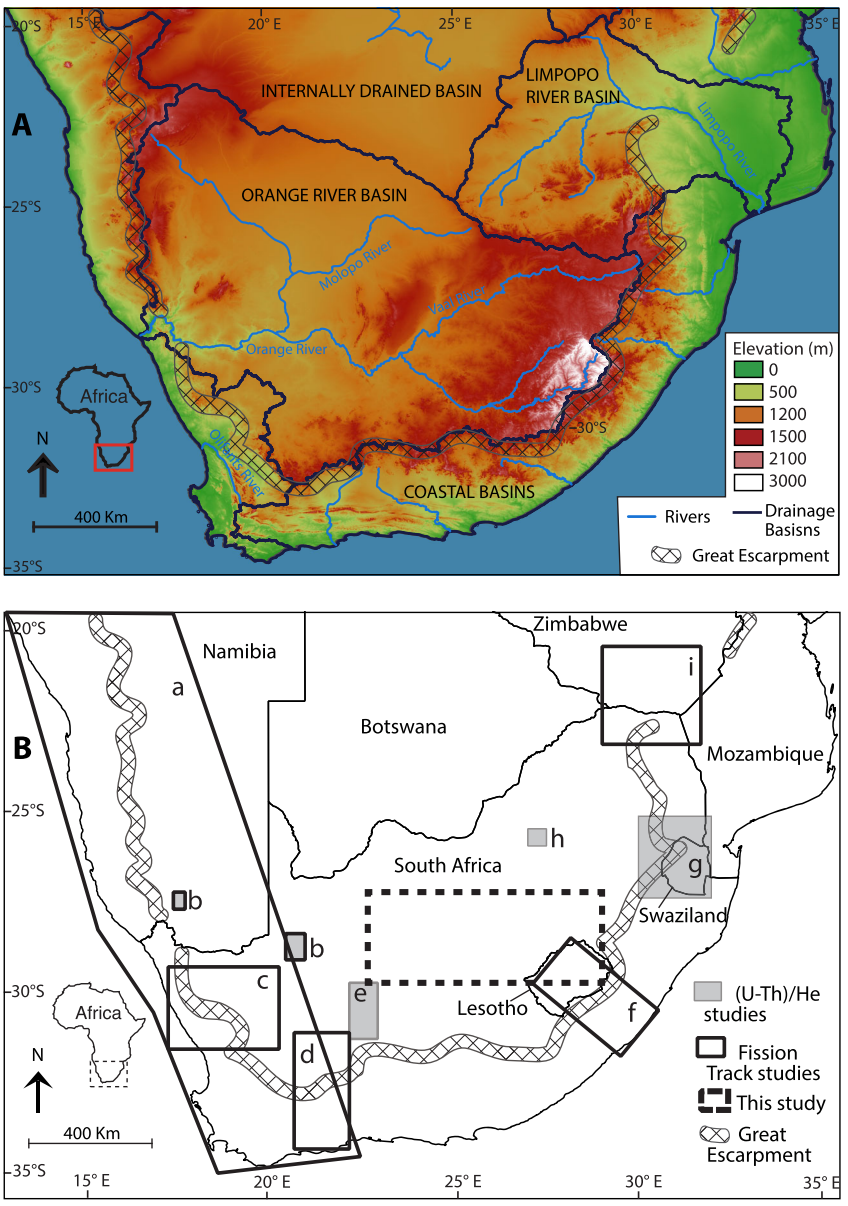

Figure 1. (a) Southern African topography showing major rivers, large-scale drainage catchments, and the Great Escarpment. (b) Locations of previous AFT and AHe studies in southern Africa. (a) *Brown et al*. [1990] and *Gallagher and Brown* [1999]. (b) *Kounov et al*. [2013]. (c) *Kounov et al*. [2009]. (d) *Tinker et al*. [2008b]. (e) *Stanley et al*. [2013]. (f) *Brown et al*. [2002]. (g) *Flowers and Schoene* [2010]. (h) *Beucher et al*. [2013]. (i) *Belton and Raab* [2010]. No prior data exist for our study area in the plateau interior.

Southern Africa is one of the most widely cited examples of elevated dynamic topography on the continents [e.g., *Lithgow-Bertelloni and Silver*, 1998; *Gurnis et al*., 2000; *Conrad and Gurnis*, 2003] (Figure 1a). The southern African Plateau has an average elevation of ~1000 m, roughly 500 m higher than is typical for cratonic areas such as this one [*Nyblade and Robinson*, 1994]. The region has not been affected by tectonic convergence since at least the late Paleozoic, when marine sedimentary rocks indicate that the plateau was at sea level. These rocks were subsequently elevated, requiring a mechanism besides plate convergence and crustal thickening to explain their uplift. Southern Africa is positioned over one of the largest low seismic velocity anomalies in the lower mantle, commonly called the "African superplume" [e.g., *Ritsema*, 1999; *Ni et al*., 2002]. Together these observations have led some to suggest that the southern African Plateau is dynamically supported by upwelling from this anomaly [*Lithgow-Bertelloni and Silver*, 1998; *Gurnis et al*., 2000; *Conrad and Gurnis*, 2003; *Braun et al*., 2014]. Presently, southern Africa is surrounded by the divergent

margins of the south Atlantic and Indian Oceans. It has been argued that Africa has been relatively stationary with respect to the underlying mantle and the Earth's spin axis since ~30 Ma [*Burke and Wilson*, 1972].

Because of the widespread notion that southern Africa may be dynamically supported, there is intense interest in its elevation change history owing to its potential utility for calibrating dynamic models [e.g., *Gurnis et al*., 2000]. However, the antiquity of this topography is debated. Many workers suggest a Mesozoic origin based largely on thermochronologic data interpretation [e.g., *Brown et al*., 2002; *van der Beek et al*., 2002; *Doucouré and de Wit*, 2003; *Tinker et al*., 2008b, 2008a *Flowers and Schoene*, 2010] (Figure 1b). Others interpret it as a more recent feature, <30 Ma, based mostly on broad-scale erosion surface correlations [*Du Toit*, 1933; *King*, 1948; *Partridge and Maud*, 1987; *Burke and Gunnell*, 2008], although these surfaces have not been dated directly.

In addition, even in southern Africa, where some of the strongest arguments for dynamically supported topography are made, discriminating between topographic support from the lithosphere versus that from the deeper mantle is not clear-cut. Southern Africa was affected by two post-200 Ma large igneous provinces (LIPs) associated with the breakup of Gondwana, as well as by two major pulses of Cretaceous kimberlite magmatism. These magmatic events appear to have perturbed the lithosphere [e.g., *Bell et al*., 2003; *Griffin*, 2003], and thus are potential sources of topographic change. The contribution of the lithospheric mantle to topography is difficult to quantify, and often highly simplified in mantle dynamic models. A more thorough investigation of these lithospheric effects is important to isolate the extent to which the topography in southern Africa is truly dynamically sourced.

In this study, we address these problems by integrating (U-Th)/He dating of kimberlites across the interior of the southern African Plateau with the shallow and deep records contained within these pipes (Figure 2). Our previous work showed that this approach is uniquely powerful for tightly bracketing continental erosion phases that can then be linked with the lithospheric mantle record preserved in mantle xenolith suites in the same pipes [*Stanley et al*., 2013]. Our initial study was in an off-craton region of the plateau, and documented an interval of accelerated Cretaceous erosion contemporaneous with lithospheric heating, thinning, and metasomatism, suggesting that these lithospheric thermochemical changes contributed to surface uplift and erosion. This same mantle modification event, however, is less extensive and pervasive on-craton [*Bell et al*., 2003; *Griffin*, 2003; *Kobussen et al*., 2009]. Here we expand our previous work with an additional suite of 19 samples from 15 kimberlite pipes in an east-west transect across the Kaapvaal craton to constrain the erosion histories and patterns across the southern African Plateau interior. We then compare these on-craton results with those from off-craton, consider how the differences in lithospheric modification affected these surface histories, and evaluate the implications for the lithospheric and deeper dynamic contributions to the topographic history of the southern African Plateau.

2. Background

2.1. Topographic Setting

The topography of southern Africa is dominated by the southern African Plateau. The low-relief plateau interior is locally elevated to >3000 m, with an average elevation of >1000 m (Figure 1a). The plateau is surrounded on three sides by the high relief "Great Escarpment," where the elevation drops rapidly to near sea level. Anomalous elevations are postulated to extend into the bathymetry of the southeastern Atlantic Ocean, and together these areas have been termed the African Superswell [*Nyblade and Robinson*, 1994]. The first-order basin and swell structure of the whole of the African continent has fascinated workers since it was first presented by *Holmes* [1944]. Studies combining gravity anomalies and topography have suggested that these structures may not be completely isostatically supported [*Hartley et al*., 1996].

The majority of the plateau interior is drained by the Orange River, which enters the south Atlantic on the west coast at the South Africa-Namibia border (Figure 1). Many workers argue for significant drainage reorganization since the breakup of Gondwana [*Dingle and Hendey*, 1984; *de Wit*, 1999; *Moore and Larkin*, 2001; *Goudie*, 2005]. Suggested mechanisms for these reorganizations include uplift related to the emplacement of LIPs [*Cox*, 1989], dynamic topography [*Braun et al*., 2014], and NE-SW trending flexural epeirogenic uplift axes roughly corresponding to drainage divides [*Moore et al*., 2009].

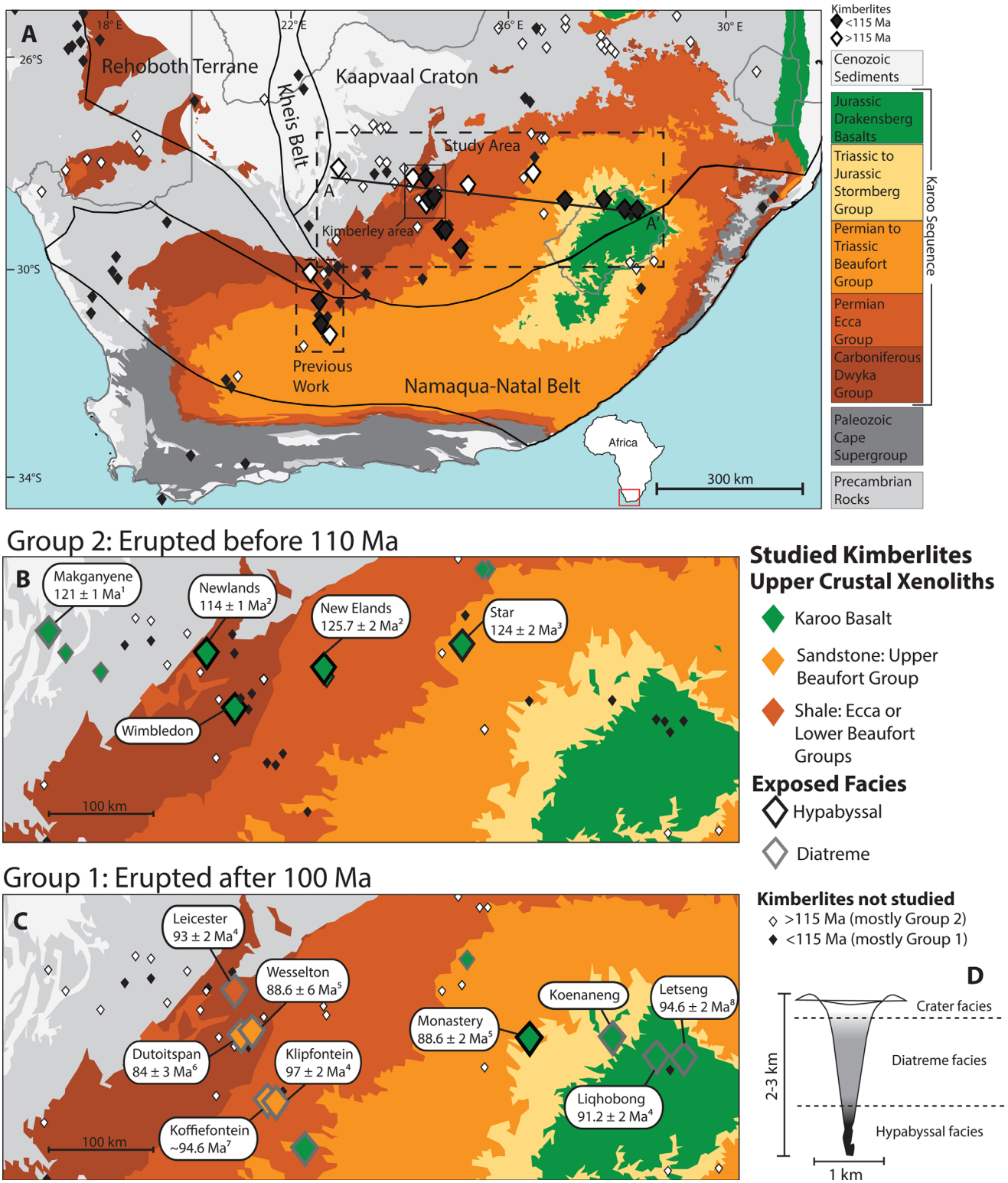

Figure 2. (a) Simplified geologic map of southern Africa showing dated kimberlite locations [*Jelsma et al.*, 2009]. Enlarged kimberlite symbols show those investigated in this study or in our previous work [*Stanley et al.*, 2013]. Gray lines indicate national boundaries. (b and c) Enlarged view of the study area showing the (b) Group 2 and (c) Group 1 kimberlites and their published eruption ages. Largest kimberlite symbols denote those dated by AHe in this study, while medium-sized symbols are those where the upper crustal xenoliths have been studied. Studied kimberlites are coded by the youngest Karoo Basin rocks entrained as upper crustal xenoliths in the pipes, as well as by the kimberlite facies exposed at the surface today [*Hanson et al.*, 2009]. [1]Rb-Sr mica, [*Brown et al.*, 1989]. [2]Rb-Sr mica, whole rock, [*Smith et al.*, 1985a]. [3]K-Ar mica [*Macintyre and Dawson*, 1976]. [4]U-Pb perovskite, [*Griffin et al.*, 2014]. [5]U-Pb perovskite [*Batumike et al.*, 2008]. [6]Rb-Sr mica, whole rock [*Allsopp and Barrett*, 1975]. [7]U-Pb zircon [*Davis*, 1977]. [8]U-Pb zircon [*Allsopp et al.*, 1989]. (d) Simplified cross section through a typical southern African kimberlite [after *Hawthorne*, 1975].

2.2. Geologic Setting

The basement rocks of southern Africa consist of the Archean Kaapvaal and Zimbabwe cratons sutured by the 2.6–2.7 Ga [*Kreissig et al*., 2001] Limpopo mobile belt (Figure 2a). These cratons are surrounded by other Proterozoic mobile belts and terranes, including the Paleoproterozoic Rehoboth Terrane on the western margin and Mesoproterozoic Namaqua-Natal metamorphic province to the southwest of the Kaapvaal Craton (Figure 2a). Overlying these basement rocks are locally preserved a variety of Precambrian sedimentary and volcanic sequences.

The Phanerozoic geology of southern Africa is dominated by the ~300–180 Ma Karoo Basin sedimentary units, volcanic rocks of the Karoo LIP, and Cenozoic Kalahari deposits (Figure 2a). The Karoo sedimentary rocks once covered the majority of southern Africa and still extend over much of the landscape [*Catuneanu et al*., 2005]. The basal sequences of the main Karoo Basin were deposited in a foredeep related to subduction in the south along the paleo-Pacific margin of Gondwana [*Catuneanu et al*., 2005]. The remnants of this orogeny are present in southern Africa as the Cape Fold Belt. The Karoo sequence in the main Karoo basin consists of the glacially derived marine ~300–290 Ma Dwyka Group, followed by deep to shallow marine sequences of the ~290–255 Ma Ecca Group, and the terrestrial Beaufort (~255–238 Ma) and Stormberg (~230–183Ma) Groups [*Catuneanu et al*., 2005]. Karoo basin deposition terminated with the extrusion of the Drakensberg Group lavas of the Karoo LIP at 183 Ma [*Duncan et al*., 1997]. Our study area is an E-W transect across the southern Kaapvaal Craton in an area that was once covered by the Karoo sequence and where portions of the Karoo Basin are still exposed today.

The African Plate was affected by several episodes of intraplate magmatism during the Mesozoic, the most extensive of which was the Karoo LIP. The Karoo LIP is associated with the breakup of Gondwana and the opening of the Indian Ocean, with rapid emplacement of its basaltic rocks at ~183 Ma [*Svensen et al*., 2012]. Karoo igneous rocks extend over most of southern Africa and into adjacent areas of Antarctica. Other Cretaceous LIPs include the Etendeka LIP in Namibia dated at ~132 Ma [*Renne et al*., 1996], and the ~100–94 Ma Agulhas oceanic plateau located off the southern coast [*Parsiegla et al*., 2008]. Southern Africa was also pierced by numerous kimberlites and related alkaline magmas, including two significant pulses in the Cretaceous, as discussed further in section 3.

2.3. Previous Low-Temperature Thermochronometry

Apatite fission-track (AFT) and apatite (U-Th)/He (AHe) are two low-temperature thermochronometers that have been applied in southern Africa. These methods are sensitive to temperatures of ~60–110°C [*Green et al*., 1986] and ~30–90°C [*Farley*, 2000; *Flowers et al*., 2009], respectively. Assuming a typical cratonic geotherm of 20°C/km and a surface temperature of 20°C appropriate for southern Africa, the AFT and AHe techniques can constrain erosion magnitudes of 2–4.5 km and 0.5–3.5 km, respectively. In this paper, we use "unroofing" to refer to erosion magnitudes, and "uplift" or "surface uplift" to refer to elevation gain above sea level. Although surface uplift can induce accelerated erosion, this need not always be the case, and additional assumptions must be made to infer that erosion was a consequence of elevation gain.

The majority of low-temperature thermochronometry studies from the southern African Plateau are AFT investigations located seaward of the Great Escarpment (Figure 1b) [*Brown et al*., 1990; *Gallagher and Brown*, 1999; *Brown et al*., 2002; *Tinker et al*., 2008b; *Kounov et al*., 2009]. Most of these studies focused specifically on the evolution and retreat of the passive margin after Gondwana breakup. AFT dates from these areas are typically Cretaceous, with most studies interpreting periods of rapid cooling and erosion at 140–120 Ma and 100–80 Ma, associated with Cretaceous surface uplift [*Brown et al*., 1990; *Tinker et al*., 2008b; *Kounov et al*., 2009]. The more limited AHe data acquired in Precambrian basement rocks near the plateau margins yield dates that are dominantly 110–80 Ma, contemporaneous with the younger erosion pulse detected by AFT [*Flowers and Schoene*, 2010; *Kounov et al*., 2013]. These two erosion pulses have been linked with the timing of rapid deposition in the basins off the South African coasts [*Tinker et al*., 2008a; *Rouby et al*., 2009; *Guillocheau et al*., 2012]. Using numerical modeling and AFT data, some workers have inferred that the southeast African margin was already elevated above sea level prior to Gondwana breakup at ca. 180 Ma [*van der Beek et al*., 2002].

In contrast to the abundance of studies seaward of the escarpment, there is little thermochronology data from the low-relief plateau interior where denudation magnitudes were lower (Figure 1b). The handful of available AFT dates from the plateau interior are older than 200 Ma, suggesting that the magnitude of post-

Jurassic exhumation in the plateau interior is generally too low to be detected by AFT [*Gallagher and Brown*, 1999]. To address this, recent studies have utilized the AHe technique both because of its lower temperature sensitivity and because recent methodological advances now allow AHe thermochronometry to resolve more detailed thermal histories than possible previously [*Flowers et al*., 2009; *Brown et al*., 2013]. *Stanley et al*. [2013] used AHe dating of kimberlites from a plateau interior location to constrain a regional unroofing pulse at ~100–90 Ma as well as a more localized Cenozoic erosion phase, and linked these results with information gleaned from mantle xenoliths in the same pipes. In addition, AHe data for a sample from a plateau interior borehole records cooling between 150 and 100 Ma [*Beucher et al*., 2013], likely due to erosion.

3. Coupling the Deep and Shallow Records of Kimberlites

3.1. Kimberlite Magmatism and the Mantle Xenolith Record in Southern Africa

Numerous kimberlites and related alkaline magmas were emplaced in southern Africa from ~1800 to 45 Ma [*Jelsma et al*., 2004]. These eruptions occurred preferentially along northeastward trending corridors [*Jelsma et al*., 2004, 2009; *Moore et al*., 2008]. Southern Africa experienced two compositionally distinct pulses of Cretaceous kimberlite magmatism. The Group 2 kimberlites, sometimes termed orangeites, erupted from ~200–110 Ma, with an eruption peak at ~140–120 Ma, whereas the Group 1 kimberlites erupted dominantly from 100 to 80 Ma [*Moore et al*., 2008; *Jelsma et al*., 2009]. While Group 1 and Group 2 technically refer to the composition of the kimberlite, here we use them more loosely to refer to the two main Cretaceous eruption pulses. In both groups, emplacement age tends to young from NE to SW [*Moore et al*., 2008; *Jelsma et al*., 2009]. However, the two groups have distinct major element, trace element, and Sr, Nd, Hf, and Pb isotopic compositions [*Smith*, 1983; *Smith et al*., 1985b; *le Roex*, 1986; *Nowell et al*., 2004; *Becker and le Roex*, 2006]. Both groups were generated by low-degree melting of enriched peridotite. Based on major and trace element modeling, many suggest that the older Group 2 kimberlites were derived from melting of the metasomatized lithospheric mantle [e.g., *Smith*, 1983; *Tainton and McKenzie*, 1994; *Becker and le Roex*, 2006; *Griffin et al*., 2014]. In this case, enrichment is of calc-alkaline character and is inferred to have occurred significantly (>400 Ma) earlier than the generation of the Group 2 kimberlites themselves [*Becker and le Roex*, 2006; *Griffin et al*., 2014]. In contrast, the major and trace element geochemistry of the Group 1 kimberlites has been interpreted to indicate derivation from a source in the convecting mantle that interacted to varying degrees with the subcontinental lithosphere [e.g., *Heaman*, 1989; *Skinner*, 1989; *Tappe et al*., 2011; *Griffin et al*., 2014]. Others have argued for a two stage melting process involving both a lithospheric and sublithospheric source similar to that of ocean island basalts [*le Roex*, 1986; *Janney et al*., 2002; *le Roex et al*., 2003]. Multiple pulses of Cretaceous kimberlite magmatism within the same geographic area mean that the composition of kimberlites and their lithospheric mantle xenolith suites capture a record of mantle processes over the time span of kimberlite emplacement.

The mantle xenolith suite from southern Africa is perhaps the most extensively studied in the world. Mantle xenoliths entrained by kimberlites, as well as xenocryst and kimberlite whole-rock and mineral compositions, have been used to characterize the continental lithosphere beneath southern Africa. While the Kaapvaal Craton is underlain by cold, depleted lithosphere, many workers recognize a Cretaceous modification event during which the lithosphere was heated, metasomatized, and variably thinned [*Konzett et al*., 2000; *Bell et al*., 2003; *Griffin*, 2003; *Schmitz and Bowring*, 2003; *Kobussen et al*., 2008, 2009; *Janney et al*., 2010]. How pervasive and permanent these modifications were is more ambiguous, because kimberlites only bring a limited sampling of the lithosphere to the surface and can locally alter their immediate mantle surroundings. However, it appears that these changes were more dramatic and infiltrated to shallower levels off-craton and in areas of preexisting structures or weaknesses than on-craton [*Bell et al*., 2003; *Kobussen et al*., 2009; *Griffin et al*., 2014]. Additionally, low heat flow measurements suggest that concentrations of U, Th, and K in the lithosphere must be low [*Rudnick et al*., 1998], suggesting relatively limited metasomatism within the craton.

3.2. The Surface Records Contained in Kimberlites

The form of kimberlites and the upper crustal xenoliths they contain can be used to constrain the timing and magnitudes of surface erosion. Kimberlite pipes in southern Africa have a typical morphology (Figure 2d), with an ~300 m thick crater facies followed by a 1–3 km diatreme facies, and then a root zone of hypabyssal facies kimberlite [*Hawthorne*, 1975; *Mitchell*, 1995; *Field and Scott Smith*, 1999; *Sparks et al*., 2006].

Most South African kimberlites exhibit diatreme or hypabyssal facies at the surface, suggesting appreciable postemplacement unroofing.

Due to the complex nature of kimberlite eruptions, diatremes can contain downrafted crustal clasts from stratigraphic layers present at time of eruption that were since eroded away, recording the stratigraphy present when the kimberlite was emplaced. Studies of these crustal xenoliths suggest that the Karoo flood basalts covered the entire southern Kaapvaal craton when the Group 2 pipes erupted, but that the basalts were removed from the southwestern craton by the time the Group 1 pipes were emplaced (Figures 2b and 2c) [*Hanson et al*., 2009]. In the southern craton, the basalts are now only preserved in the Lesotho remnant on the eastern margin of the craton (Figure 2). This spatial pattern of basalt xenoliths has been explained in terms of a scarp retreat model, with an eastward retreating scarp removing the basalt cover over time [*Hanson et al*., 2009].

Information from the kimberlite pipes and the projected stratigraphic thicknesses of the Karoo basin have been used to estimate erosion magnitudes in the Kimberley area. The initial estimate from *Hawthorne* [1975] suggested 900–1900 m of post-90 Ma erosion based on sill emplacement depths and extent of host rock diagenesis. This estimate was subsequently refined to ~1350 m since 120 Ma and ~850 since 90 Ma from stratigraphic thickness estimates and sedimentary xenoliths [*Hanson et al*., 2009].

4. Apatite (U-Th)/He Thermochronology

4.1. Strategy and Samples

AHe thermochronology is sensitive to ~30–90°C, depending on the radiation damage accumulated in the apatite crystal [*Farley*, 2000; *Shuster et al*., 2006; *Flowers et al*., 2009]. The effect of radiation damage is to increase the apatite He retentivity such that apatites with higher U and Th concentrations, and therefore higher damage levels, will have higher effective closure temperatures than those grains with lower U and Th. For thermal histories in which apatites spent substantial time in the 30–90°C temperature range, the result is a positive correlation between AHe date and effective uranium concentration (eU, [U] + 0.235[Th]) [*Flowers et al*., 2007]. Working with kimberlitic apatites is advantageous because they are typically low in eU and therefore sensitive to lower temperatures and lower unroofing magnitudes than apatites of more typical composition. In addition to radiation damage, AHe dates are influenced by grain size and fragmentation effects [*Reiners and Farley*, 2001; *Brown et al*., 2013].

We obtained samples of kimberlites and crustal xenoliths from a suite of 15 pipes in an ~600 km long west to east transect across the southern Kaapvaal Craton (Figure 2a). Here the Cretaceous kimberlites are excellent targets for AHe because they are younger than the surrounding Precambrian basement rocks, and therefore record shorter and simpler thermal histories. In southern Africa, the multiple pulses of kimberlite magmatism mean that there are sets of kimberlites that begin recording the denudation histories at different times. The cooling histories of kimberlites of different ages can therefore be used to tightly constrain intervals of erosion [e.g., *Stanley et al*., 2013].

The sample transect extends from ~200 km west of Kimberley to the highlands of Lesotho (Figure 2a and supporting information Table S1). The strategy was to sample pairs of Group 2 (120–140 Ma emplacement ages) and Group 1 (85–100 Ma emplacement ages) kimberlites located in close proximity to one another along the transect to best bracket the erosion history since kimberlite eruption. In practice, this was only possible in some locations because not all kimberlites yielded apatite of sufficient quality for AHe analysis and because of a paucity of Group 2 kimberlites in the far eastern portion of the transect. All the sampled Group 2 kimberlites contain clasts of the Karoo basalt and exhibit diatreme or hypabyssal facies at the surface (Figure 2b and supporting information Table S1) [*Hanson et al*., 2009]. Of the sampled Group 1 kimberlites, those in the western study area do not contain Karoo basalt clasts, while those in the center and eastern portions of the transect either contain basalt clasts or erupt through the present-day basalt exposure (Figure 2c and supporting information Table S1) [*Hanson et al*., 2009].

Samples were either collected at the kimberlite itself or obtained from the Mantle Room collection at the University of Cape Town. When possible, we targeted apatites separated from both the kimberlite matrix and crustal xenoliths entrained in the pipe. This was done because kimberlites do not always yield adequate apatite, and because using apatites from both lithologies can yield a wider range of apatite eU from a single

locality, which can help to further refine the thermal history as discussed below. Previous work indicates that clasts in kimberlites attain temperatures of 225 to >925°C during kimberlite eruption [*Pell et al*., 2015], which is hot enough to reset the apatite (U-Th)/He system during the eruption process. Thus, apatites from crustal clasts should record similar histories to the kimberlitic apatites regardless of the initial depth of derivation of the crustal xenolith.

4.2. Results

We acquired (U-Th)/He data for 97 individual apatite grains and 11 multigrain apatite aliquots on 19 samples from 15 different kimberlite pipes. Five samples are crustal granitoid or dolerite clasts contained in the pipe, and 14 samples are the kimberlite matrix. The 15 kimberlite pipes include five Group 2 and 10 Group 1 kimberlites. Most kimberlites have at least five single-grain analyses. The sample dates are reported as the mean and the 1σ standard deviation when the standard deviation is <20% of the mean. Samples with >20% dispersion are reported as a range of single grain dates. All data are reported in supporting information Table S2. Detailed information about methods is in supporting information Text S1.

Apatite eU varies from <5 to 160 ppm, with most grains <60 ppm. Many kimberlite apatites are characterized by low eU (<30 ppm). While these low eU values are useful for their low temperature sensitivity, it also means that the apatite dates are more vulnerable to other sources of dispersion such as implantation from high eU grain boundary coatings [*Murray et al*., 2014] or neighboring grains with high eU [*Spiegel et al*., 2009]. If AHe data for a sample are affected by these phenomena, a U-shaped date-eU correlation is expected [*Murray et al*., 2014]. We observe this U-shaped pattern in several of our samples, and therefore have chosen not to interpret grains with <5 ppm eU because they are often highly dispersed and display this pattern (supporting information Figure S1). Data for these grains are reported in the data table, but not included in the average sample date and not shown in plots.

Many of the apatites are fragments with one or both tips broken. Fragmentation can affect AHe dates for certain thermal histories, but this effect is far less significant than the influence of radiation damage [*Beucher et al*., 2013; *Brown et al*., 2013]. We evaluated our results to determine whether we could exploit the fragmentation effect to better restrict the thermal history simulations discussed in section 5. Although we suspect that fragmentation may be a secondary source of dispersion in our data, it does not appear to affect the results in a systematic manner (supporting information Figure S2). We therefore do not consider this effect further.

The AHe results for Group 2 and Group 1 kimberlites are shown separately in Figures 3 and 4. We further divided the kimberlites into subgroups based on their geographic location and AHe dates. Figures 3a and 4a show the sample locations and AHe dates. Figures 3b and 4b are plots of individual AHe date versus longitude, with the kimberlite emplacement age range shown as a light gray band. The analyses are color-coded for eU because the data span in many samples is correlated with eU and thus can be explained by the radiation damage effect on apatite He retentivity. Individual AHe dates range from significantly younger than eruption to overlapping eruption age, depending on the kimberlite. Grains derived from the kimberlite matrix and the crustal clasts appear to behave similarly and overlap in age when both are present in one kimberlite (Figures 3b, 4b and supporting information Figure S3). All data except for those apatites with <5 ppm eU are shown on the AHe-date eU plots in Figures 3 and 4. The AHe date-eU plots for each subgroup are shown with their associated thermal history simulations, which are discussed in the next section (Figures 3c–3j and 4c–4q).

The Group 2 kimberlite data set includes seven samples from five kimberlites, and is subdivided into three subgroups (Figure 3). The first subgroup consists of the two Group 2 kimberlites closest to the edges of the Karoo Basin, Makganyene, and Star, located at the west and east ends of the transect, respectively (Figure 3a). These kimberlites yielded mean dates of 98.8 ± 15 and 92.7 ± 13 Ma, which are younger than eruption (Figures 3b and 3c), with a possible weak positive date-eU correlation in Makganyene (Figure 3c). Note that Star yielded only low eU grains so the shape of its date-eU correlation is not well constrained. We chose to group it with Makganyene based on the similarity of their thermal history simulation results (see below). The two kimberlites from the Kimberley area, Newlands, and Wimbledon, compose the second subgroup (Figure 3a). These data show overlapping strong positive AHe date-eU correlations that range from ~60 to 140 Ma, with the oldest AHe dates overlapping the eruption age (Figures 3b and 3f). In the central craton, New Elands has a mean AHe date of 68 ± 9 Ma, significantly younger than its eruption age (Figures 3a and

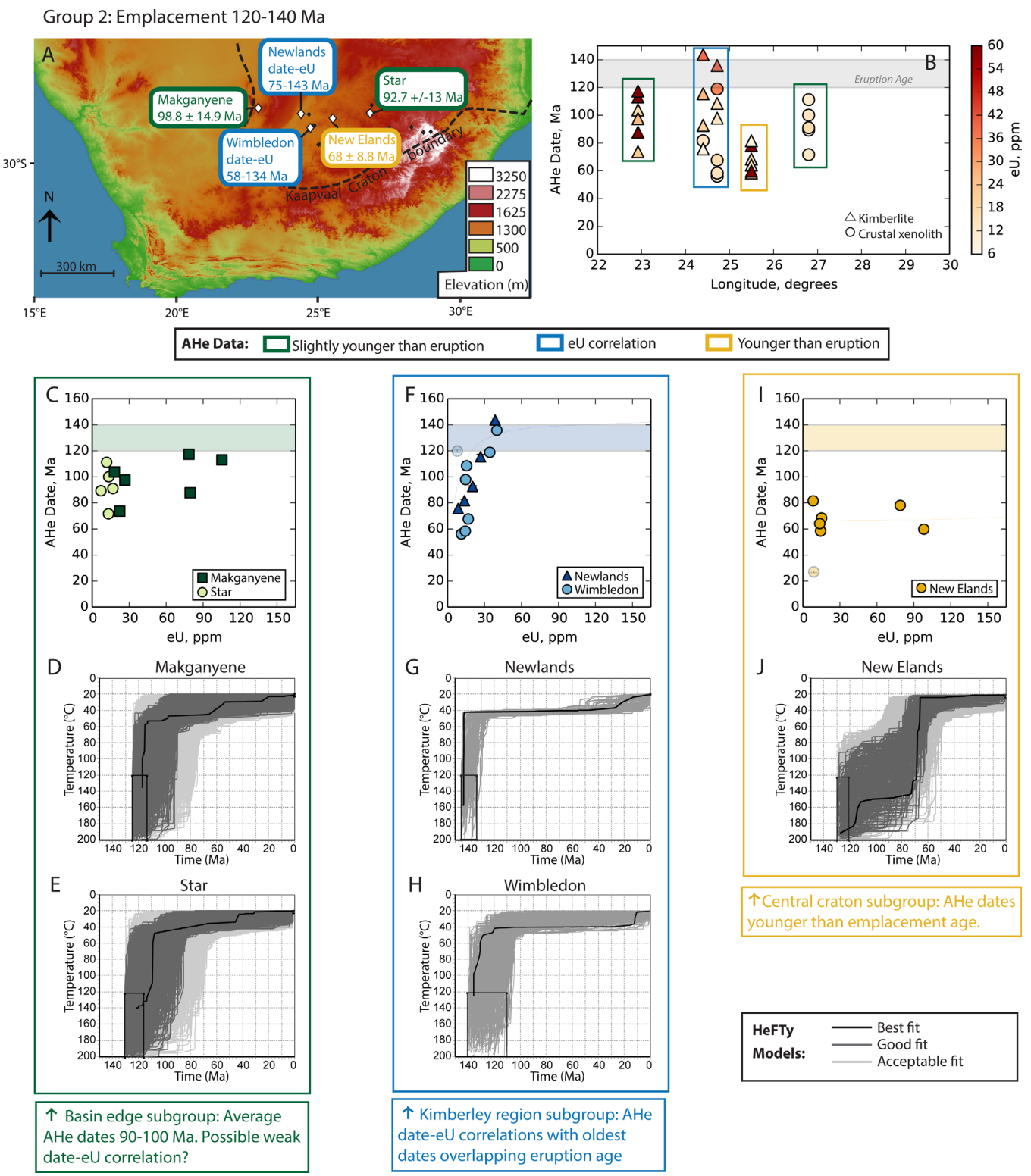

Figure 3. AHe data and thermal history simulations for the Group 2 kimberlites. (a) Map with location and average AHe date or range of dates for each sample. Colors indicate how the AHe data relate to the eruption age. (b) Individual grain AHe date plotted against sample longitude. Symbol shape indicates whether the apatite was from the kimberlite matrix or a crustal granitoid clast. Symbol color indicates eU value. Gray bar represents eruption age range for these kimberlites. (c–e) Date-eU plot (c) and thermal history simulations (d and e) for kimberlites in the basin edge subgroup. (f–h) Date-eU plot (f) and thermal history simulations (g and h) for kimberlites in the Kimberley region subgroup. (i and j) Date eU plot (i) and thermal history simulations (j) for the central craton subgroup. Grayed out symbols on date-eU plots were not used in the HeFTy simulations.

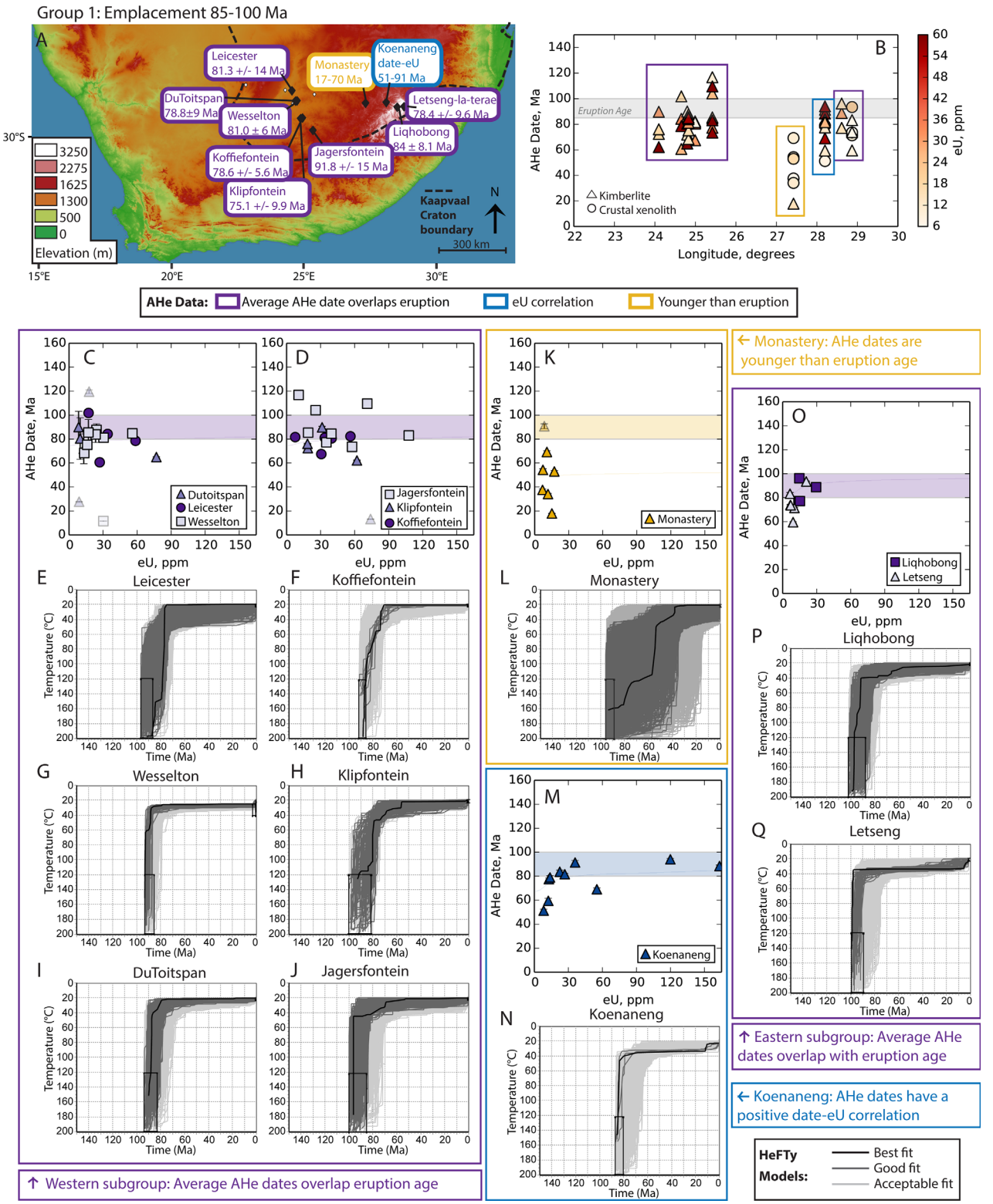

Figure 4. AHe data and thermal history simulations for the Group 1 kimberlites. (a) Map with location and average AHe date or range of dates for each sample. Colors indicate how the AHe data relate to the eruption age. (b) Individual grain AHe date plotted against sample longitude. Symbol shape indicates whether the apatite was from the kimberlite matrix or a crustal granitoid clast. Symbol color indicates eU value. Gray bar represents eruption age range for these kimberlites. (c–j) Date-eU plots (c and d) and thermal history simulations (e–j) for kimberlites in the western subgroup. (k and l) Date-eU plot (k) and thermal history simulations (m) for the Monastery kimberlite. (m and n) Date-eU plot (m) and thermal history simulations (n) for the Koenaneng kimberlite. (o–q) Date-eU plot (o) and thermal history simulations (p and q) for the eastern subgroup. Grayed out symbols on date-eU plots were not used in the HeFTy simulations.

3b). Its relatively young, uniform dates over a broad eU span distinctly differ from the data patterns in the other Group 2 kimberlites (Figure 3i).

The Group 1 kimberlite results include data for 12 samples from 10 kimberlites, which we divided into four subgroups (Figure 4). The western subgroup includes six kimberlites (Figures 4a and 4b). For clarity, these data are split into two date-eU plots consisting of kimberlites from the Kimberley area (Wesselton, DuToitspan, and Leicester, Figure 4c) and those southeast of Kimberley (Koffiefontein, Klipfontein, and Jagersfontein, Figure 4d). AHe dates for all of these western kimberlites overlap or are slightly younger than eruption, with no date-eU correlations (Figures 4a–4d). In the central craton, there are two subgroups each containing one kimberlite, which contrast with the western subgroup because they show at least some apatite grains that are systematically younger than eruption age. Apatites from the Monastery kimberlite are all low eU ($<$18 ppm), younger than eruption, and have high He data dispersion, with individual grain dates ranging from 17 to 70 Ma (Figure 4k). Koenaneng apatites have a wider range of eU, with the low eU grains as young as 51 Ma and the high eU grains overlapping eruption (Figure 4m). The eastern subgroup of kimberlites includes Letseng and Liqhobong, which sit in the highlands of Lesotho within the Karoo basalt remnant (Figures 2 and 4a). These kimberlites yielded apatites with a limited eU range and AHe dates that overlap or are just younger than eruption (Figures 4b and 4o).

5. Thermal History Simulations

A large number of thermal histories can satisfy any given AHe date, so thermal history simulation software was used to limit the possible thermal histories to those which best replicate the data and are consistent with geologic constraints. The 15 kimberlites were simulated individually using the inverse modeling capabilities of the HeFTy program [*Ketcham*, 2005] and the radiation damage accumulation and annealing model (RDAAM) for apatite He diffusion kinetics [*Flowers et al*., 2009]. HeFTy simulates random time-temperature (tT) paths conforming to defined thermal history constraints and finds "good" and "acceptable" fit thermal histories that simultaneously satisfy the date, eU, and equivalent spherical radius (r) for each sample [*Ketcham*, 2005]. The "good" fits are intended to be good to the limit of statistical precision, and defined such that the mean of goodness-of-fit statistics assessed is 0.5, and the minimum is $1/(N+1)$, where N is the number of statistics used [*Ketcham et al*., 2009]. For each sample between 10,000 and 100,000 random tT paths were simulated to constrain the full range of "good-fit" histories. The only constraints imposed on the HeFTy models were that the rock was $>$120°C when the kimberlite erupted, where the eruption age is based on published emplacement dates (supporting information Table S1), and that the surface temperature is 20°C at the end of the simulation. For HeFTy simulations, individual grains were binned based on their eU values and the average of each bin was modeled, allowing us to capture the date-eU trends in the data (for more information see supporting information Text S2).

Figures 3 and 4 show all the thermal history simulation results. On each tT plot, the black box represents the eruption date, with the "best," good, and acceptable fit histories in black, dark gray, and light gray, respectively. The Group 2 kimberlites at the edges of the basin, Makganyene (Figure 3d) and Star (Figure 3e), show similar families of good-fit thermal histories that are consistent with their postemplacement AHe dates. In both cases, the paths do not cool to surface temperatures until 100 Ma or later, well after eruption, and the majority of cooling taking place by 85 Ma. In contrast, the AHe data for the Kimberley area kimberlites (Figure 3g-Newlands; Figure 3h-Wimbledon) yield tT paths that cool rapidly to $\sim$40°C after eruption, and then reside at this temperature until cooling to the surface in the Cenozoic. This extended interval in the partial retention zone can explain the date-eU correlations of these samples. New Elands in the central craton (Figure 3j) shows yet a different history, due to AHe dates that are substantially younger than emplacement over their entire eU span. The good-fit histories require that the rocks be $>$60°C until 80 Ma, with most paths cooling to $<$40°C by 60 Ma, suggesting rapid cooling between 80 and 60 Ma.

The Group 1 kimberlites in the western (Figures 4e–4j) and eastern (Figures 4p–4q) subgroups have similar thermal histories that cool rapidly to surface temperatures after eruption, consistent with their AHe dates that mostly overlap with the kimberlite emplacement age. The distinction between these two subgroups is based on their location and geology rather than the cooling histories, because the eastern subgroup

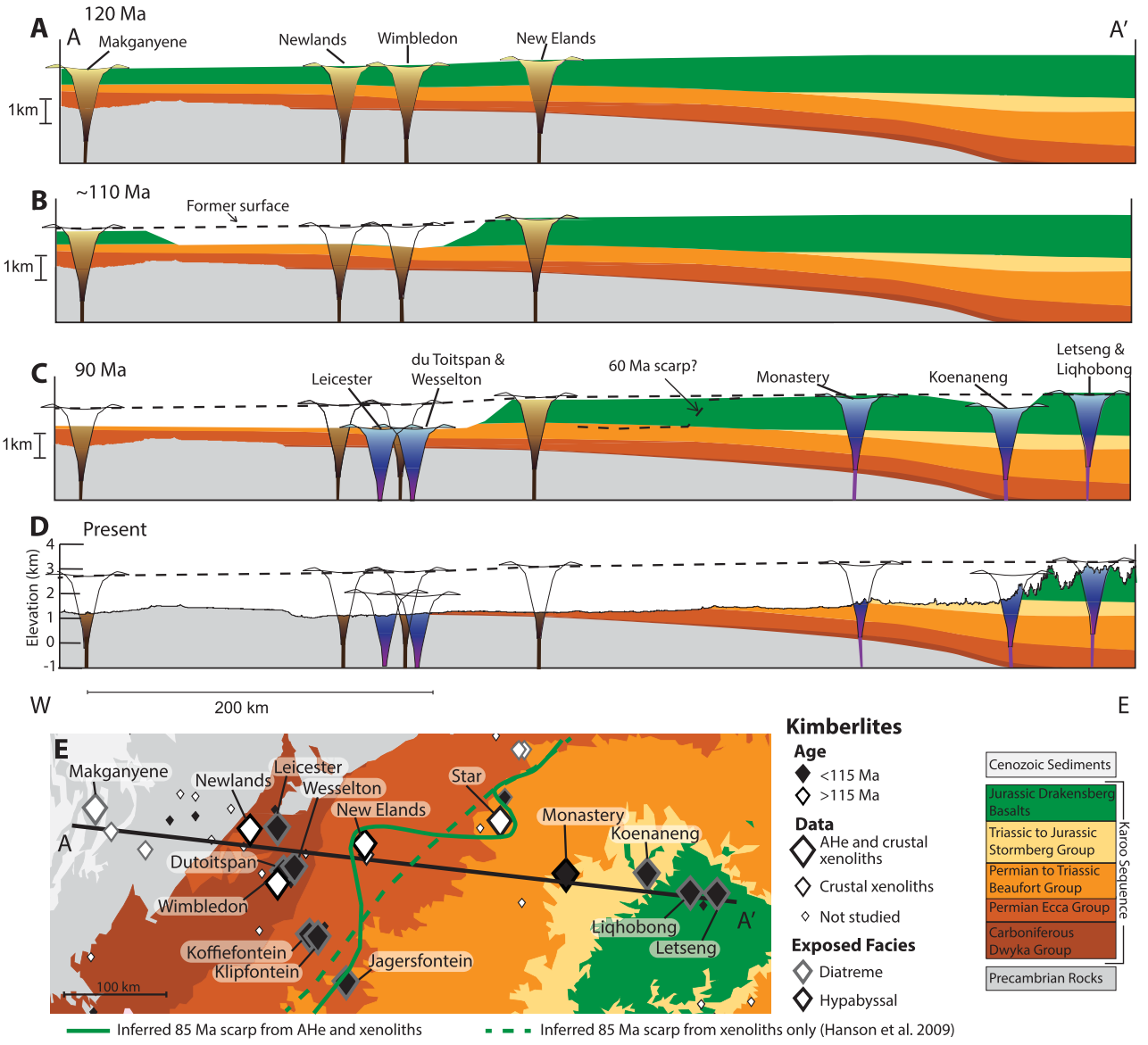

Figure 5. (a–d) Preferred unroofing model for the southern Kaapvaal Craton. See text for details. (e) Scarp front position at ~85 Ma based on thermochronometry and crustal xenoliths (solid line, this study) and crustal xenoliths only [dashed line, *Hanson et al.*, 2009].

presently crops out within the Karoo basalt remnant (Figure 2). The central craton shows cooling histories different than the eastern and western subgroups (Figures 4k–4n). The most distinctive is Monastery (Figure 4l), which, based on the good-fit paths, does not cool to surface temperatures until after 60 Ma. Monastery's cooling paths are perhaps most similar to the Group 2 kimberlite New Elands (Figure 3h), which also is located in the central transect. Koenaneng (Figure 4n) also does not cool to surface temperatures immediately, with the good-fit paths requiring the sample to remain at >30°C for an extended interval.

6. Discussion

6.1. Preferred Unroofing Model for the Southern Kaapvaal Craton

We reconstructed the history and patterns of erosion across our ~600 km long plateau interior transect using stratigraphic constraints, kimberlite pipe geometry, and the thermal history simulation results. To accomplish this, we first produced a cross section that restored the eroded section from postulated sedimentary thicknesses based on previous studies [*Hawthorne*, 1975; *Johnson et al.*, 1996; *Hanson et al.*, 2009]. Figure 5 shows our preferred unroofing model. All kimberlites were projected on the cross section except

those >50 km from the section line because of appreciable south-north sedimentary thinning rates in the Karoo Basin. Unroofing magnitudes are based on the good-fit results of the HeFTy models assuming a 20°C/km geothermal gradient and 20°C surface temperature, assumed sedimentary thicknesses, and exposed kimberlite facies. Additional details about reconstruction methods are in supporting information Text S3.

At 120 Ma, when the Group 2 kimberlites peaked in magmatic activity (Figure 5a), xenoliths suggest that the Karoo basalts still covered the entire transect. The modeled tT paths for Kimberley area Group 2 kimberlites suggest fast cooling to moderate temperatures after eruption (Figures 3g and 3h). From the thermal history results alone, we cannot distinguish cooling by unroofing from cooling of the kimberlite magma to ambient temperatures. However, in the Kimberley area we interpret that basalt cover removal between 120 and ~110 Ma contributed to cooling (Figure 5b) because basalt xenoliths show that the basalt was still present at the time of kimberlite emplacement. In contrast, we infer that Makganyene farther west retained significant cover until ~100–90 Ma (Figure 5b), because its cooling phase is somewhat younger (Figure 3f).

At ~90 Ma, when the Group 1 kimberlites peak in magmatic activity (Figure 5c). In the western part of the transect the basalt cover was removed before Group 1 kimberlite eruption because these pipes lack basalt xenoliths. The AHe dates of these western Group 1 kimberlites roughly overlap with eruption age, limiting the magnitude of postemplacement erosion. However, these kimberlites do contain Beaufort Group xenoliths suggesting that some sedimentary rock cover was removed from this region post-90 Ma. Group 1 kimberlites in the central and eastern parts of the transect contain basalt xenoliths, demonstrating that basalt cover was still present there at 90 Ma. Between 90 Ma and present, the basalt and some of the underlying units were eroded from the central craton, as recorded by AHe dates substantially younger than eruption from the Group 2 New Elands kimberlite and the Group 1 Monastery kimberlite (Figures 3i, 3j and 4k, 4l). The data suggest earlier cooling at New Elands, the westernmost of these two pipes, than at Monastery, farther east, consistent with a scarp retreating eastward across the craton between 90 Ma and the present.

Broadly speaking this wave of erosion, likely representing a scarp, can be tracked across our study area. At ~110 Ma it may have initiated in the Kimberley area, perhaps along a river valley, as recorded by the Group 2 kimberlites there (Figure 5b). The subgroup of Group 2 kimberlites on the basin edges (Makganyene, Figure 3d and Star, Figure 3e) record cooling that can be explained by scarp migration between 110 and 90 Ma. The western subgroup of Group 1 kimberlites erupted after the scarp passed through this region, and thus their AHe dates overlap with eruption (Figures 4c and 4d). The Group 1 and Group 2 kimberlites in the central craton record the passage of this scarp after 90 Ma, with AHe results that postdate eruption. The eastern subgroup of Group 1 kimberlites (Figures 4o–4q) sit at higher elevations within the present-day exposure of the Karoo basalt and have yet to see this wave of erosion, and therefore have cooling dates coeval with eruption (Figure 5d).

The combination of AHe thermochronometry and the crustal xenolith information constrains details of the scarp front sinuosity that are not detectable from the crustal xenoliths alone. The inferred scarp position at ~85 Ma is shown in Figure 5e, where the dashed line represents the location inferred from the crustal xenoliths only [*Hanson et al*., 2009], and the solid line shows our refined interpretation that also exploits our AHe data. The sinuosity in the scarp is based on the thermal histories from the Group 2 Star kimberlite (Figure 3e), which suggest that this pipe's main cooling phase was complete by 85 Ma. We did not project Star onto the cross section in Figure 5 because it is farther from the section line and it records this secondary complexity about the scarp front location. At the Group 2 New Elands kimberlite, southwest of Star, the main cooling phase began no earlier than 80 Ma, suggesting that basalt cover persisted until that time. Thus, we interpret the earlier cooling event at Star to record scarp retreat before New Elands. The Group 1 Jagersfontein kimberlite, located south of New Elands (Figure 2c and supporting information Table S1), contains basalt xenoliths, indicating that basalt cover was present when Jagersfontein erupted at ~90 Ma. However, this pipe's AHe dates overlap with eruption, suggesting basalt removal shortly after pipe emplacement (Figures 4d and 4j). Together this information implies that the scarp position was likely quite close to Jagersfontein at 85 Ma (Figure 5e). This scarp front sinuosity is not unexpected given the irregularity of the modern scarp at the base of the Lesotho highlands.

Another example of uneven topography is likely recorded by the four Group 1 kimberlites in the eastern portion of the transect. The Koenaneng AHe data show a date-eU correlation, suggesting some posteruption cooling, which the tT simulations imply was <15°C (Figures 6m and 6n). Koenaneng sits just west of

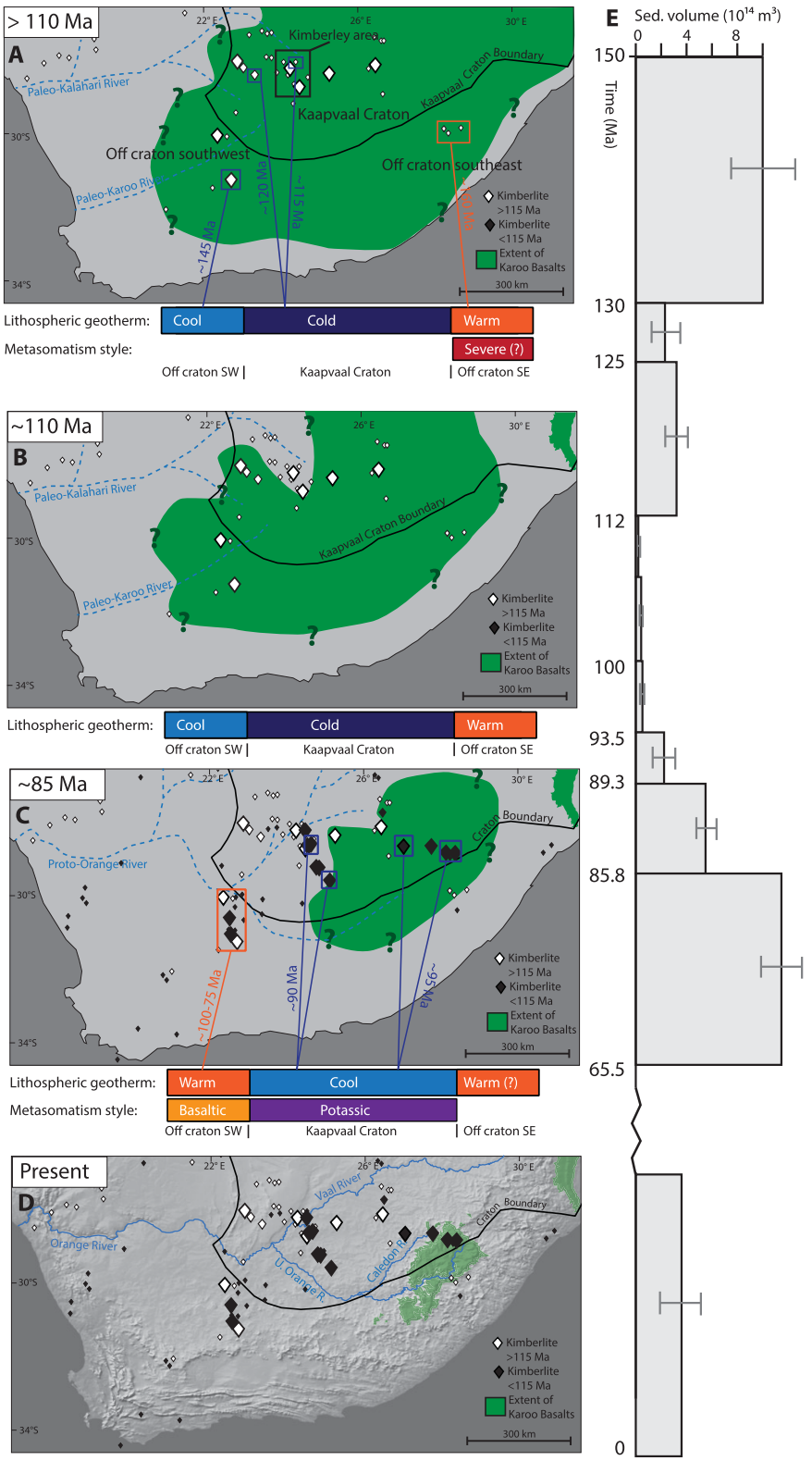

Figure 6. Reconstruction of Karoo basalt extent and simplified representation of the thermochemical state of the lithosphere before (a) 110 Ma, at (b) ~110 Ma, at (c) ~85 (Ma), and (d) at present. See text for full discussion. (e) Accumulated volume of terrigeneous sediment in the marine Orange River Basin from *Guillocheau et al.* [2012].

the modern escarpment at the base of the Karoo basalts, >800 m lower than Letseng and Liqhobong to the east (Figure 5d). The scarp must have retreated past this point after Koenaneng's eruption, removing the basalt cover, with the AHe data limiting the erosion magnitude to ~750 m. Monastery, just to the west, shows still younger AHe dates than Koenaneng (Figure 4k), despite the similarity of these pipes in terms of elevation and presumed initial thickness of stratigraphic cover (Figure 5). The simplest explanation for the differences in AHe data and thermal histories between Monastery and Koenaneng is that at least some topography existed at the ~90 Ma time of eruption. There is >1000 m of relief within the present-day basalt remnant, so it is reasonable to envision that Koenaneng erupted into an incised valley (Figure 5c), perhaps the proto-valley for the present-day Caledon River that runs nearby.

6.2. Plateau Interior Erosion History, River Drainage Evolution, and Offshore Sediment Flux

Our thermochronometry study is the first to encompass such a large tract of the southern African Plateau interior, therefore adding significant information about the Cretaceous and younger erosion history on the plateau itself (Figure 1b). The majority of previous thermochronometry investigations were from the plateau margins or coastal plain, and interpreted two major cooling phases at 140–120 Ma and 100–80 Ma [*Gallagher and Brown*, 1999; *Brown et al.,* 2002; *Tinker et al*., 2008a; *Kounov et al*., 2009; *Flowers and Schoene*, 2010]. Our results for Group 2 kimberlites in the Kimberley area may detect the end of the 120–140 Ma erosion episode, but our data set dominantly records the spatial progression of the younger erosion phase across the plateau.

Previous AFT studies pointed out that the Cretaceous cooling pulses correspond to intervals of increased sediment volume in the offshore record [*Tinker et al*., 2008b,a]. The Orange Basin, which would be the depocenter for material eroding from our study area, records high sediment flux and volume from ~150 to 112 Ma and from ~93 to 65 Ma [*Guillocheau et al*., 2012]. Both of these sediment influx pulses, but especially the younger one, are coincident with the erosion intervals documented by our data in the plateau interior (see sediment volume summary in Figure 6). Evidence from Orange Basin stratigraphy, as well as paleochannel gravel deposits, have been used to argue for a number of major drainage reorganizations of the Orange River and its tributaries [*Dingle and Hendey*, 1984; *Partridge and Maud*, 1987; *de Wit*, 1999; *Moore and Moore*, 2004; *Stevenson and McMillan*, 2004; *de Wit et al*., 2009]. Our data cannot fully differentiate between these drainage reconstructions, but our preferred erosion history is consistent with the drainage model of *de Wit et al*. [2009] (key aspects this of drainage model are shown in Figure 6). This reconstruction honors evidence for a northwestward flowing Cretaceous-aged river that was eroding diamond-bearing kimberlites, including perhaps the Newlands kimberlite as recorded in a deposit ~90 km northwest of Newlands. This history is compatible with our erosion model (Figure 5), which suggests that the Newlands and Wimbledon kimberlites eroded shortly after eruption.

Our data detect a wave of erosion on the Kaapvaal Craton that took ~60 Ma to migrate from west to east across ~400 km of the plateau interior. This protracted erosion history is different from the distinct pulses of erosion detected on the coastal plain [e.g., *Brown et al.,* 2002; *Tinker et al*., 2008a], as well as from the more regional, accelerated unroofing phase at ~110–90 Ma detected by AHe in the off-craton plateau interior [*Stanley et al*., 2013]. The latter event is approximately contemporaneous with the onset of the major unroofing wave seen on-craton, but the on-craton signal is more spatially variable than that off-craton. If these erosion patterns are a consequence of surface uplift, then the differences on-craton and off-craton suggest that the deeper lithospheric structure may be important in the manifestation of surface uplift.

6.3. Relationships Between the Erosion History and On-Craton Versus Off-Craton Lithospheric Mantle Modification

The southern African Plateau consists of different blocks of Precambrian lithosphere, with complexity in the lithospheric architecture visible in present-day seismic images. Figure 7 is a tomographic image produced by the Kaapvaal Project that displays the *P* wave velocity perturbations at 150 km depth [*James et al*., 2001; *Fouch et al*., 2004a]. The Archean Kaapvaal Craton mostly shows higher *P* wave speeds, suggesting colder, thicker lithosphere. The off-craton regions, including the Proterozoic Namaqua-Natal Belt where our previous study area was located [*Stanley et al*., 2013], show slower *P* wave speeds, likely indicating warmer, less chemically depleted, and/or more metasomatized lithosphere (Figure 7).

Previous work indicates that these different lithospheric domains were variably modified by a wave of Cretaceous lithospheric heating and metasomatism thought to originate from the same source but manifested differently depending on the lithospheric structure [*Bell et al*., 2003; *Griffin*, 2003; *Kobussen et al*., 2009].

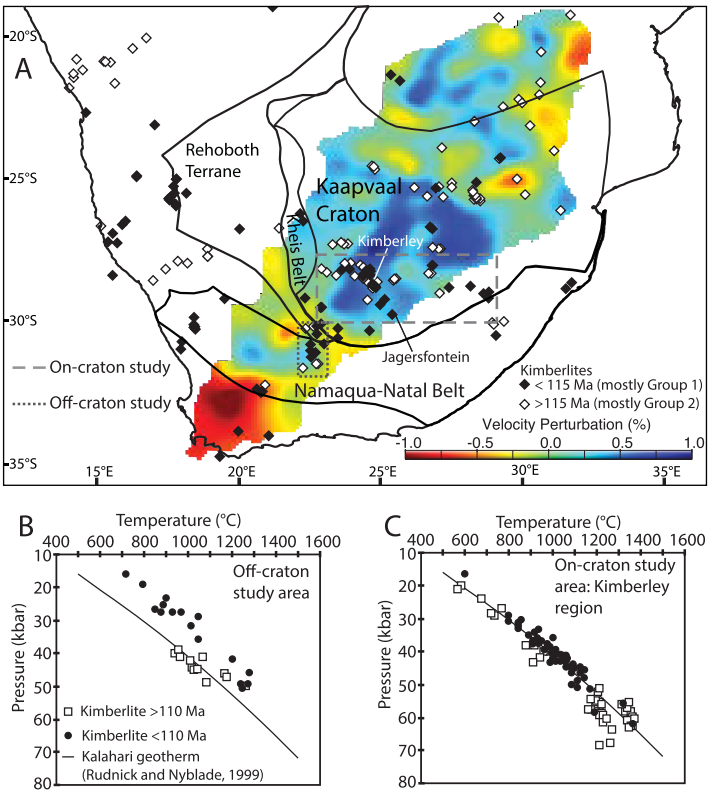

Figure 7. (a) *P* wave tomographic model of southern Africa at 150 km depth showing the variability in lithospheric structure today [after *Fouch et al*., 2004a,b]. Also shown are the surface boundaries of the Kaapvaal Craton and the Proterozoic Namaqua-Natal mobile belt, the kimberlites with published ages [*Jelsma et al*., 2009], and the locations of our on-craton and off-craton study areas. (b and c) Mantle xenolith-based geotherm from (b) the off-craton southwest study area and (c) the on-craton Kimberley region [after *Bell et al*., 2003]. Thermobarometry was calculated using the two-pyroxene method [*Brey and Köhler*, 1990]. The off-craton array shows a much larger increase in temperature between the older kimberlites (white squares) and the younger kimberlites (black circles).

Importantly, these thermochemical changes can modify the lithospheric density structure, such that we might expect a different surface response in the off-craton region where the lithospheric mantle was more strongly modified than on-craton where the lithosphere was less-affected by the same event. Here we first summarize the changes in the lithospheric mantle during the Cretaceous and then explore relationships with the surface history.

Warming of the mantle lithosphere has been documented between emplacement of the Group 2 and Group 1 pipes at many localities by thermobarometry on mantle xenoliths and xenocrysts. For the off-craton regions, *Bell et al*. [2003] inferred a wave of lithospheric heating that swept from southeast to northwest across southern Africa, starting by ~160 Ma southeast of the craton, occurring between 140 and 100 Ma southwest of the craton, and affecting the region northwest of the craton by 60 Ma.

Within the craton there is evidence from garnet xenocryst thermobarometry that the mantle geotherm warmed from the time of Group 2 to Group 1 kimberlite eruption, though less significantly than off-craton [*Griffin*, 2003]. *Kobussen et al*. [2009] concluded that metasomatism by silicate melt produced heating whereas hydrous mineral metasomatism did not, thus restricting the heating to the lower reaches of the cratonic lithosphere and producing a stronger heating signal in the off-craton and cratonic margin kimberlite suites. Thermobarometry of xenoliths from the Finsch and Newlands Group 2 kimberlites is consistent with somewhat cooler mantle beneath these pipes at the time of their eruption than beneath Group 1 kimberlites [*Menzies et al*., 1999; *Gibson et al*., 2008; *Lazarov et al*., 2009]. However, data from the Finsch suite are restricted mostly to the deeper levels of the lithosphere (Figure 7b). Somewhat complicating the interpretation of mantle temperature differences as a temporal effect within the craton is the proposed existence of heterogeneously distributed zones of Mesozoic and older mantle metasomatism, such as in the Kimberley region [*Begg et al*., 2009; *Griffin et al*., 2009]. Such zones may be warmer due to locally higher heat production. On-craton xenolith geotherms documenting hotter than average temperatures at >50 kbar pressure are present in the Group 1 kimberlites near the craton edge (Lesotho and Jagersfontein) and less obvious in the craton interior (Figure 7c, Kimberley region pipes). This pattern suggests that while not immune to thermal disturbance, the Kaapvaal cratonic mantle was less affected by thermal modification than the surrounding Proterozoic terranes, which is consistent with the modern seismic tomography (Figure 7a). In some regions, particularly off-craton, this thermochemical modification of the lithospheric mantle is thought to be accompanied by 30–40 km of lithospheric thinning [*Kobussen et al*., 2008; *Janney et al*., 2010].

In addition to the mantle xenoliths, accessory mineral U-Pb thermochronometry on lower crustal xenoliths suggests Mesozoic warming of the lower crust by as much as 200–300°C, with more significant off-craton

than on-craton heating [*Schmitz and Bowring*, 2003]. These data imply that the warming affected much of the lithospheric column, particularly in the off-craton and craton-margin areas.

Garnet xenocryst and xenolith data also suggest that the lithospheric mantle was metasomatized between the eruption of Group 2 and Group 1 kimberlites, with different metasomatic styles on-craton and off-craton. Off-craton in the Proterozoic terranes, garnet xenocrysts record heating accompanied by "basaltic-style" metasomatism by silicate melt addition. The xenocrysts derived from on-craton kimberlites display chemical evidence for "potassic-style" metasomatism, caused by addition of potassium rich fluids [*Kobussen et al*., 2009]. Textural evidence also exists for metasomatism from "MARID" (Mica Amphibole Rutile Ilmenite Diopside) xenoliths and veins in peridotite xenoliths from both on-craton and off-craton kimberlites [*Dawson and Smith*, 1977]. Zircons from MARID xenoliths yield dates that overlap with the age of kimberlite magmatism (∼110–85 Ma), which was interpreted to indicate metasomatism at this time [*Konzett et al*., 2000]. In the off-craton suite, xenoliths from many of the younger kimberlites show evidence for phlogopite, clinopyroxene, and spinel replacing garnet [*Janney et al*., 2010], interpreted as an isobaric metasomatic reaction in the presence of potassium-rich melts or fluids [*Erlank et al*., 1987].

We summarize the temporal and spatial relationships between the surface and deep histories of the plateau interior in Figure 6, which shows three key Cretaceous snapshots plus the modern state. Each plot displays the extent of the Karoo basalt cover and the character of regional mantle modification at that time. The reconstruction of basalt cover is well constrained in our study areas (Figures 6b and 6c). Elsewhere the depicted extent is more schematic, as denoted by question marks, and estimated based on the locations of preserved Karoo basalts and on the shape of the modern Karoo Basin. We assume that erosion broadly took place by scarp retreat controlled by river incision, and that the rate of erosion by the scarp was likely slower as the scarp moved closer to the drainage divide. Regional mantle geotherms based on xenoliths are broadly divided into "cold," "cool," and "warm." A "cold" geotherm is a typical cratonic geotherm similar to other archetypal cratons such as Slave and Siberia. A "cool" geotherm is slightly elevated, but overlaps with the "Kalahari Geotherm" of *Rudnick and Nyblade* [1999], which was based on xenoliths derived from the Group 1 (∼90 Ma) kimberlites from the Kaapvaal and Zimbabwe Cratons. A "warm" geotherm is significantly elevated above the cratonic geotherm by ∼100°C at all depths. "Basaltic-style" or "potassic-style" metasomatism is defined based on the garnet xenocryst chemistry as described above [*Kobussen et al*., 2009]. "Severe" metasomatism denotes significant addition of clinopyroxene, phlogopite, and other metasomatic minerals to the xenoliths [*Janney et al*., 2010].

Before ∼110 Ma, the Karoo basalts covered most of the landscape (Figures 5a and 6a). The Group 2 kimberlites had erupted and contain Karoo basalt xenoliths [*Kobussen et al*., 2009]. Thermobarometry on the mantle xenolith suites indicates that the on-craton lithosphere from 160 to 120 Ma was characterized by a cold cratonic geotherm, with lithospheric thickness estimates of 210–250 km [*Michaut et al*., 2007], although by ∼114 Ma warmer temperatures are recorded in the deep (>50 kbar) xenoliths in some cases. Xenoliths from the off-craton southwest region show a cool geotherm overlapping with the slightly warmer Kalahari geotherm [*Bell et al*., 2003]. In contrast, the mantle xenolith derived geotherm southeast of the craton is much warmer [*Bell et al*., 2003; *Janney et al*., 2010], with evidence for severe metasomatism [*Janney et al*., 2010]. While the exact timing of metasomatism in these eastern pipes is not well constrained, it is consistent with being caused by the impinging of the Karoo plume and Gondwana breakup [*Janney et al*., 2010], which also likely increased the geotherm.

AHe thermochronometry suggests that by ∼110 Ma, the basalt cover was eroding on-craton around the Kimberley area (Figures 5b and 6b). In contrast, basalt cover persisted southwest of the craton, suggesting that significant erosion had not yet initiated there [*Stanley et al*., 2013]. The on-craton erosion phase at this time appears to be spatially focused along paleorivers rather than of a regional character, although we cannot preclude additional more widespread erosion of lesser magnitude. One possibility is that the lithospheric heating east of the craton elevated the surface there, contributed to westward tilting of the entire region, and caused erosion to begin along major river valleys farther west. This erosion event subsequently propagated upstream owing to the greater erosional efficiency of rivers at base level where the drainage area is largest (Figure 6b). Such a continent-wide tilting was suggested based on a landscape evolution model that aimed to replicate the pattern of sediment flux in the Orange River Basin [*Braun et al*., 2014]. This on-craton erosion interval coincides with accelerated erosion from ∼120 to 140 Ma documented by

AFT studies on the coastal plain [*Brown et al.*, 2002; *Tinker et al.*, 2008b]. The transition from rift to drift in the opening of the south Atlantic occurred at ~130 Ma [*Brown*, 1995; *McMillan*, 2003], and may also have helped trigger for this Early Cretaceous erosion event.

At ~90 Ma, the Group 1 kimberlites peaked in magmatic activity. By ~85 Ma, the basalt cover was removed from the off-craton southwest region by a significant regional unroofing phase [*Stanley et al.*, 2013]. The on-craton erosion signal is more spatially variable, with basalt cover only partially removed by ~85 Ma, and a sinuous scarp front present in the central craton (Figure 6c). The on-craton mantle xenoliths and xenocrysts show that the lithosphere here was still cool, though possibly slightly warmer than during the Group 2 kimberlite magmatism, and associated with "potassic-style" metasomatism (Figures 7c and 6c) [*Rudnick and Nyblade*, 1999; *Bell et al.*, 2003; *Kobussen et al.*, 2009]. The off-craton southwest kimberlites, however, show a warmer geotherm associated with "basaltic-style" metasomatism (Figures 7b and 6c) [*Bell et al.*, 2003; *Kobussen et al.*, 2009].

By the present time (Figure 6d), the scarp has retreated to the far eastern craton. There are no on-craton lithospheric mantle xenolith constraints after 90 Ma, but seismic tomography suggests that significant heterogeneity in the lithospheric architecture remains today, with thick lithosphere in the western craton, thinner lithosphere in the off-craton southwest region, and elevated temperatures to the southeast of the craton presumably due to thinned lithosphere (Figure 7a) [*James et al.*, 2001; *Fouch et al.*, 2004b; *Chevrot and Zhao*, 2007].

6.4. Implications for Mantle Sources of Topographic Change

The major goal of this study was to document the erosion history and patterns across the southern African Plateau interior and assess how they are related to mantle sources of uplift. By comparing two regions affected by different degrees of Cretaceous lithospheric modification, we can better isolate the lithospheric contribution to topography and evaluate possible dynamic buoyancy sources for the elevations. Mid-Cretaceous modification of the southern African mantle lithosphere was more pervasive off-than on-craton, even though the modification event is thought to stem from the same source [*Bell et al.*, 2003; *Kobussen et al.*, 2009]. In both regions, the modification may be heterogeneously distributed and accentuated in zones of previous tectonic activity. We recognize that interpreting what the erosion patterns signify for the detailed surface uplift history is not necessarily straightforward, because unroofing is not a perfect proxy for surface uplift and erosion is inherently a mixture of signals from surface processes and the deeper uplift sources. Nonetheless, the on-craton and off-craton regions appear to be characterized by different erosion signatures, and these correlate with the contrast in the extent of lithospheric alteration (Figure 6c). We therefore interpret causative links between surface uplift that was partly induced by lithospheric modification and the erosion history revealed by our data set. Note that our work can only detect erosion phases younger than our studied kimberlites. It does not preclude earlier erosion or uplift phases that might have been associated with other events such as Jurassic Karoo basalt heating and magmatism.

The post-Jurassic erosion history of the southern Kaapvaal craton was dominated by protracted west-to-east scarp retreat that continued until at least 60 Ma (Figure 5). The spatial pattern of unroofing suggests that erosion in the central craton was controlled dominantly by the geometry of the Orange River drainage system. A key outcome of our on-craton study is that there was not a substantial, pronounced interval of accelerated erosion specifically coincident with the limited cratonic lithosphere modification phase in the mid-Cretaceous. This result implies that the unroofing patterns here were not strongly influenced by this lithospheric event.

In contrast, in our off-craton study area a significant, regional erosion phase from ~110 to 90 Ma is synchronous with pervasive lithospheric thermochemical modification [*Stanley et al.*, 2013]. Because we lack erosion constraints to the east and west of our off-craton transect, and this off-craton study area is more limited in spatial extent than our on-craton study, it is more difficult to determine whether an eastward retreating scarp was also important here. However, we do not detect an ~110–90 Ma erosion event of comparable size on the southern Kaapvaal craton, except at its southwestern corner just abutting the off-craton study area (Figure 6c). The on-craton xenoliths closest to the craton margins, including Jagersfontein at the southern edge, show more thermal modification at deep levels than those in the central craton [*Bell et al.*, 2003]. We suggest that pervasive lithospheric heating, metasomatism and thinning of the off-craton southwest region and adjacent craton margin contributed to surface uplift and triggered regional erosion here (Figure 7c).

Many workers have proposed that the southern Africa Plateau is dynamically supported because of its anomalous elevations [e.g., *Nyblade and Robinson*, 1994] and position over a large slow seismic anomaly in the deep mantle that could be a dynamic buoyancy source [e.g., *Lithgow-Bertelloni and Silver*, 1998; *Gurnis et al*., 2000; *Conrad and Gurnis*, 2003; *Braun et al*., 2014]. Our finding of an apparent lack of a substantial lithospheric-sourced uplift and erosion signal on-craton is consistent with this notion of a sublithospheric contribution to plateau elevations. However, the erosional response to the more severe lithospheric changes in the off-craton region suggests that lithospheric support of topography is important in some parts of the plateau. Kimberlite magmatism and lithospheric thermochemical modification possibly were induced by deeper mantle dynamic processes such as African "superplume" development [e.g., *Zhang et al*., 2010], movement of the African continent over the "superplume" [e.g., *Torsvik et al*., 2010; *Braun et al*., 2014], or hotspots moving beneath the craton [*le Roex*, 1986]. While the lithospheric and deeper sources of buoyancy may be intimately related, our work suggests that the lithosphere has an important modulating effect on the surface expression of mantle dynamics.

7. Conclusions

1. We used AHe thermochronometry, kimberlite information, and additional geologic constraints to decipher the erosion history of the southern African Plateau interior. The results document initially spatially focused erosion along river valleys, followed by eastward retreat of a scarp from ~120 to <60 Ma across ~600 km of the southern Kaapvaal Craton. At ~85 Ma, we are able to place the location of a sinuous scarp front just east of the Kimberley area with more detail than was previously known using crustal xenolith constraints alone.
2. Off-craton, regional erosion at ~110–90 Ma was contemporaneous with lithospheric heating and modification, suggesting that lithospheric processes contributed to topographic change. In contrast, on-craton erosion at this time was more spatially variable and accompanied by more subtle lithospheric modification, suggesting perhaps a more important contribution from deeper dynamic buoyancy sources to its elevations. These relationships suggest that surface uplift was spatially variable, with differing influences from lithospheric and deeper dynamic sources.
3. The differences in the surface and lithospheric histories on-craton and off-craton highlight the importance of lithospheric architecture for the manifestation of the surface response to deeper mantle processes. This is especially important to consider for regions with thick, complex lithosphere.

Acknowledgments
Data supporting Figures 3 and 4 can be found in the supporting information Table S2. This work was supported by NSF grant EAR-0951518 and EAR-1126991 to R.M.F. and a NSF Graduate Research Fellowship to J.R.S. We thank John Gurney and Steve Richardson at the University of Cape Town for access to samples from the mantle room collection. We also thank Chairty Mampa and Andrew Rogers at Petra Diamonds; Sentle Hlajoane; Bob Burrell at Letseng Diamonds; and Sebastian Tappe, Ferdi Winters, and Andrew Webster at De Beers for assistance regarding kimberlites. Many thanks to Maarten de Wit, Jock Robey, Jay Barton, Lew Ashwal, Sue Webb, Maria Shipapo, and Warren Miller for insightful discussions and assistance with fieldwork. Thoughtful reviews by Philip Janney and Rick Carlson helped improve the quality of this manuscript.

References

Allsopp, H. L., and D. R. Barrett (1975), Rb-Sr age determinations on South African kimberlite pipes, *Phys. Chem. Earth*, *9*, 605–617.

Allsopp, H. L., J. W. Bristow, C. B. Smith, R. Brown, A. J. W. Gleadow, J. D. Kramers, and O. G. Garvie (1989), A summary of radiometric dating methods applicable to kimberlites and related rocks, in *Proceedings of the Fourth International Kimberlite Conference*, vol. 1, edited by J. Ross, pp. 343–357, Geol. Soc. of Australia Carlton, Perth, Australia.

Ault, A. K., R. M. Flowers, and S. A. Bowring (2013), Phanerozoic surface history of the Slave craton, *Tectonics*, *32*, 1066–1083, doi:10.1002/tect.20069.

Batumike, J. M., W. L. Griffin, E. A. Belousova, N. J. Pearson, S. Y. O'Reilly, and S. R. Shee (2008), LAM-ICPMS U-Pb dating of kimberlitic perovskite: Eocene-Oligocene kimberlites from the Kundelungu Plateau, D.R. Congo, *Earth Planet. Sci. Lett.*, *267*(3–4), 609–619, doi:10.1016/j.epsl.2007.12.013.

Becker, M., and A. P. le Roex (2006), Geochemistry of South African on-and off-craton, Group I and Group II kimberlites: Petrogenesis and source region evolution, *J. Petrol.*, *47*(4), 673–703.

Begg, G. C. et al. (2009), The lithospheric architecture of Africa: Seismic tomography, mantle petrology, and tectonic evolution, *Geosphere*, *5*(1), 23–50, doi:10.1130/GES00179.1.

Bell, D. R., M. D. Schmitz, and P. E. Janney (2003), Mesozoic thermal evolution of the southern African mantle lithosphere, *Lithos*, *71*(2–4), 273–287, doi:10.1016/S0024-4937(03)00117-8.

Belton, D. X., and M. J. Raab (2010), Cretaceous reactivation and intensified erosion in the Archean-Proterozoic Limpopo Belt, demonstrated by apatite fission track thermochronology, *Tectonophysics*, *480*(1–4), 99–108, doi:10.1016/j.tecto.2009.09.018.

Beucher, R., R. W. Brown, S. Roper, F. Stuart, and C. Persano (2013), Natural age dispersion arising from the analysis of broken crystals. Part II: Practical application to apatite (U-Th)/He thermochronometry, *Geochim. Cosmochim. Acta*, *120*, 395–416, doi:10.1016/j.gca.2013.05.042.

Braun, J. (2010), The many surface expressions of mantle dynamics, *Nat. Geosci.*, *3*(12), 825–833, doi:10.1038/ngeo1020.

Braun, J., F. Guillocheau, C. Robin, G. Baby, and H. A. Jelsma (2014), Rapid erosion of the Southern African Plateau as it climbs over a mantle superswell, *J. Geophys. Res. Solid Earth*, *119*, 6093–6112, doi:10.1002/2014JB010998.

Brey, G. P., and T. Köhler (1990), Geothermobarometry in four-phase lherzolites. II: New thermobarmeters, and practical assessment of existing thermobarometers, *J. Petrol.*, *31*(6), 1353–1378.

Brown, L. F. (1995), *Sequence Stratigraphy in Offshore South African Divergent Basins: An Atlas on Exploration for Cretaceous Lowstand Traps by Soekor (Pty) Ltd, AAPG Stud. in Geol*., vol. 41, 184 pp., Am. Assoc. of Pet. Geol., Tulsa, Okla.

Brown, R. W., M. A. Summerfield, and A. J. W. Gleadow (2002), Denudational history along a transect across the Drakensberg Escarpment of southern Africa derived from apatite fission track thermochronology, *J. Geophys. Res.*, *107*(B12), 2350, doi:10.1029/2001JB000745.
Brown, R. W., H. L. Allsoppl, J. W. Bristow, and C. B. Smith (1989), Improved precision of Rb-Sr dating of kimberlitic micas: An assessment of a leaching technique, *Chem. Geol.*, *79*(2), 125–136.
Brown, R. W., D. J. Rust, M. A. Summerfield, A. J. W. Gleadow, and M. C. J. De Wit (1990), An early cretaceous phase of accelerated erosion on the south-western margin of Africa: Evidence from apatite fission track analysis and the offshore sedimentary record, *Int. J. Radiat. Appl. Instrum., Part D*, *17*(3), 339–350, doi:10.1016/1359-0189(90)90056-4.
Brown, R. W., R. Beucher, S. Roper, C. Persano, F. Stuart, and P. Fitzgerald (2013), Natural age dispersion arising from the analysis of broken crystals. Part I: Theoretical basis and implications for the apatite (U-Th)/He thermochronometer, *Geochim. Cosmochim. Acta*, *122*(120), 478–497, doi:10.1016/j.gca.2013.05.041.
Burke, K., and Y. Gunnell (2008), *The African Erosion Surface: A Continental-Scale Synthesis of Geomorphology, Tectonics, and Environmental Change Over the Past 180 Million Years*, *Geol. Soc. of Am.*, Boulder, Colo.
Burke, K., and J. T. Wilson (1972), Is the African Plate Stationary?, *Nature*, *239*(5372), 387–390.
Chevrot, S., and L. Zhao (2007), Multiscale finite-frequency Rayleigh wave tomography of the Kaapvaal craton, *Geophys. J. Int.*, *169*(1), 201–215, doi:10.1111/j.1365-246X.2006.03289.x.
Conrad, C. P., and M. Gurnis (2003), Seismic tomography, surface uplift, and the breakup of Gondwanaland: Integrating mantle convection backwards in time, *Geochem. Geophys. Geosyst.*, *4*(3), 1031, doi:10.1029/2001GC000299.
Cox, K. G. (1989), The role of mantle plumes in the development of continental drainage patterns, *Nature*, *342*, 873–877.
Davis, G. L. (1977), The ages and uranium contents of zircons from kimberlites and associated rocks, *Year Book Carnegie Inst. Washington*, *76*, 631–654.
Dawson, J. B., and J. V Smith (1977), The MARID (mica-amphibole-rutile-ilmenite-diopside) suite of xenoliths in kimberlite, *Geochim. Cosmochim. Acta*, *41*, 309–322.[12635294]
de Wit, M. C. J. (1999), Post-Gondwana drainage and the development of diamond placers in western South Africa, *Econ. Geol.*, *94*, 721–740.
de Wit, M. C. J., J. D. Ward, M. K. Bamford, and M. J. Roberts (2009), The significance of the cretaceous diamondiferous gravel deposit at Mahura Muthla, Northern Cape Province, South Africa, *S. Afr. J. Geol.*, *112*(2), 89–108, doi:10.2113/gssajg.112.2.89.
Dingle, R. V, and Q. B. Hendey (1984), Late Mesozoic and Tertiary sediment supply to the eastern Cape Basin (SE Atlantic) and Paleo-drainage systems in southewestern Africa, *Mar. Geol.*, *56*, 13–26.
Doucouré, C. M., and M. J. de Wit (2003), Old inherited origin for the present near-bimodal topography of Africa, *J. Afr. Earth Sci.*, *36*(4), 371–388, doi:10.1016/S0899-5362(03)00019-8.
Duncan, R. A., P. R. Hooper, J. Rehacek, J. S. Marsh, and A. R. Duncan (1997), The timing and duration of the Karoo igneous event, southern Gondwana, *J. Geophys. Res.*, *102*(B8), 18,127–18,138, doi:10.1029/97JB00972.
Du Toit, A. L. (1933), Crustal movement as a factor in the geographical evolution of South Africa, *S. Afr. Geogr. J.*, *16*(3), 4–20.
Erlank, A. J., F. G. Waters, C. J. Hawkesworth, S. E. Haggerty, H. L. Allsopp, R. S. Rickard, and M. A. Menzies (1987), Evidence for mantle metasomatism in peridotite nodules from the Kimberley pipes, South Africa, in *Mantle Metasomatism*, edited by M. A. Menzies and C. J. Hawkesworth, pp. 221–311, Academic, London, U. K.
Faccenna, C., and T. W. Becker (2010), Shaping mobile belts by small-scale convection, *Nature*, *465*(7298), 602–605, doi:10.1038/nature09064.
Farley, K. A. (2000), Helium diffusion from apatite: General behavior as illustrated by Durango fluorapatite The implied He closure temperature for *a grain, J. Geophys. Res.*, *105*(B2), 2903–2914, doi:10.1029/1999JB900348.
Field, M., and B. H. Scott Smith (1999), Contrasting geology of near-surface emplacement of kimberlite pipes in southern Africa and Canada, in *Proceedings of the Seventh International Kimberlite Conference*, edited by J. J. Gurney, et al., pp. 214–237, Red Roof Design cc, Cape Town, South Africa.
Flament, N., M. Gurnis, and R. D. Muller (2013), A review of observations and models of dynamic topography, *Lithosphere*, *5*(2), 189–210, doi:10.1130/L245.1.
Flowers, R. M., and B. Schoene (2010), (U-Th)/He thermochronometry constraints on unroofing of the eastern Kaapvaal craton and significance for uplift of the southern African Plateau, *Geology*, *38*(9), 827–830, doi:10.1130/G30980.1.
Flowers, R. M., D. L. Shuster, B. P. Wernicke, and K. A. Farley (2007), Radiation damage control on apatite (U-Th)/He dates from the Grand Canyon region, Colorado Plateau, *Geology*, *35*(5), 447–450, doi:10.1130/G23471A.1.
Flowers, R. M., R. A. Ketcham, D. L. Shuster, and K. A. Farley (2009), Apatite (U-Th)/He thermochronometry using a radiation damage accumulation and annealing model, *Geochim. Cosmochim. Acta*, *73*(8), 2347–2365, doi:10.1016/j.gca.2009.01.015.
Flowers, R. M., A. K. Ault, S. A. Kelley, N. Zhang, and S. Zhong (2012), Epeirogeny or eustasy? Paleozoic-Mesozoic vertical motion of the North American continental interior from thermochronometry and implications for mantle dynamics, *Earth Planet. Sci. Lett.*, *317–318*, 436–445, doi:10.1016/j.epsl.2011.11.015.
Fouch, M. J., D. E. James, J. C. VanDecar, and S. van der Lee (2004a), Mantle seismic structure beneath the Kaapvaal and Zimbabwe Cratons, *S. Afr. J. Geol.*, *107*, 33–44, doi:10.2113/107.1-2.33.
Fouch, M. J., P. G. Silver, D. R. Bell, and J. N. Lee (2004b), Small-scale variations in seismic anisotropy near Kimberley, South Africa, *Geophys. J. Int.*, *157*, 764–774, doi:10.1111/j.1365-246X.2004.02234.x.
Gallagher, K., and R. Brown (1999), Denudation and uplift at passive margins: The record on the Atlantic Margin of southern Africa, *Philos. Trans. R. Soc. London A*, *357*(1753), 835–859, doi:10.1098/rsta.1999.0354.
Gibson, S. A., J. Malarkey, and J. A. Day (2008), Melt depletion and enrichment beneath the western Kaapvaal Craton: Evidence from Finsch peridotite xenoliths, *J. Petrol.*, *49*(10), 1817–1852.
Goudie, A. S. (2005), The drainage of Africa since the Cretaceous, *Geomorphology*, *67*(3–4), 437–456, doi:10.1016/j.geomorph.2004.11.008.
Green, P. F., I. R. Duddy, A. J. W. Gleadow, P. R. Tingate, and G. M. Laslett (1986), Thermal annealing of fission tracks in apatite. 1: A qualitative description, *Chem. Geol.*, *59*, 237–253.
Griffin, W. (2003), The evolution of lithospheric mantle beneath the Kalahari Craton and its margins, *Lithos*, *71*(2–4), 215–241, doi:10.1016/j.lithos.2003.07.006.
Griffin, W. L., S. Y. O'Reilly, J. C. Afonso, and G. C. Begg (2009), The composition and evolution of lithospheric mantle: A re-evaluation and its tectonic implications, *J. Petrol.*, *50*(7), 1185–1204.
Griffin, W. L., J. M. Batumike, Y. Greau, N. J. Pearson, S. R. Shee, and S. Y. O'Reilly (2014), Emplacement ages and sources of kimberlites and related rocks in southern Africa: U-Pb ages and Sr-Nd isotopes of groundmass perovskite, *Contrib. Mineral. Petrol.*, *168*(1), 1032, doi:10.1007/s00410-014-1032-4.

Guillocheau, F., D. Rouby, C. Robin, C. Helm, N. Rolland, C. Le Carlier de Veslud, and J. Braun (2012), Quantification and causes of the terrigeneous sediment budget at the scale of a continental margin: A new method applied to the Namibia-South Africa margin, *Basin Res.*, *24*(1), 3–30, doi:10.1111/j.1365-2117.2011.00511.x.

Gurnis, M., J. X. Mitrovica, J. Ritsema, and H.-J. van Heijst (2000), Constraining mantle density structure using geological evidence of surface uplift rates: The case of the African Superplume, *Geochem. Geophys. Geosyst.*, *1*(7), 1020, doi:10.1029/1999GC000035.

Hanson, E. K., J. M. Moore, E. M. Bordy, J. S. Marsh, G. Howarth, and J. V. A. Robey (2009), Cretaceous erosion in Central South Africa: Evidence from upper-crustal xenoliths in kimberlite diatremes, *S. Afr. J. Geol.*, *112*(2), 125–140, doi:10.2113/gssajg.112.2.125.

Hartley, R., A. B. Watts, and J. D. Fairhead (1996), Isostasy of Africa, *Earth Planet. Sci. Lett.*, *137*, 1–18.

Hawthorne, J. B. (1975), Model of a kimberlite pipe, *Phys. Chem. Earth*, *9*, 1–15.

Heaman, L. M. (1989), The nature of the subcontinental mantle from Sr Nd Pb isotopic studies on kimberlitic perovskite, *Earth Planet. Sci. Lett.*, *92*(3), 323–334.

Holmes, A. (1944), *Principles of Physical Geology*, Thomas Nelson and Sons Ltd., Edinburgh, U. K.

James, D. E., M. J. Fouch, J. C. Vandecar, and S. Van Der Lee (2001), Tectospheric structure beneath southern Africa, *Geophys. Res. Lett.*, *28*(13), 2485–2488, doi:10.1029/2000GL012578.

Janney, P. E., A. P. Le Roex, R. W. Carlson, and K. S. Viljoen (2002), A chemical and multi-isotope study of the Western Cape olivine melilitite province, South Africa: Implications for the sources of kimberlites and the origin of the HIMU signature in Africa, *J. Petrol.*, *43*(12), 2339–2370.

Janney, P. E., S. B. Shirey, R. W. Carlson, D. G. Pearson, D. R. Bell, A. P. Le Roex, A. Ishikawa, P. H. Nixon, and F. R. Boyd (2010), Age, composition and thermal characteristics of South African off-craton mantle lithosphere: Evidence for a multi-stage history, *J. Petrol.*, *51*(9), 1849–1890, doi:10.1093/petrology/egq041.

Jelsma, H., W. Barnett, S. Richards, and G. Lister (2009), Tectonic setting of kimberlites, *Lithos*, *112*, 155–165, doi:10.1016/j.lithos.2009.06.030.

Jelsma, H. A., M. J. de Wit, C. Thiart, P. H. G. M. Dirks, G. Viola, I. J. Basson, and E. Anckar (2004), Preferential distribution along transcontinental corridors of kimberlites and related rocks of Southern Africa, *S. Afr. J. Geol.*, *107*, 301–324.

Johnson, M. R., C. J. Van Vuuren, W. F. Hegenberger, R. Key, and U. Shoko (1996), Stratigraphy of the Karoo Supergroup in southern Africa: An overview, *J. Afr. Earth Sci.*, *23*(1), 3–15.

Ketcham, R. A. (2005), Forward and inverse modeling of low-temperature thermochronometry data, *Rev. Mineral. Geochem.*, *58*, 275–314, doi:10.2138/rmg.2005.58.11.

Ketcham, R. A., R. A. Donelick, M. L. Balestrieri, and M. Zattin (2009), Reproducibility of apatite fission-track length data and thermal history reconstruction, *Earth Planet. Sci. Lett.*, *284*(3), 504–515.

King, L. C. (1948), On the ages of African land-surfaces, *Q. J. Geol. Soc.*, *416*, 439–459.

Kobussen, A. F., W. L. Griffin, S. Y. O'Reilly, and S. R. Shee (2008), Ghosts of lithospheres past: Imaging an evolving lithospheric mantle in southern Africa, *Geology*, *36*(7), 515–518, doi:10.1130/G24868A.1.

Kobussen, A. F., W. L. Griffin, and S. Y. O'Reilly (2009), Cretaceous thermo-chemical modification of the Kaapvaal cratonic lithosphere, South Africa, *Lithos*, *112*, 886–895, doi:10.1016/j.lithos.2009.06.031.

Konzett, È., A. Armstrong, and D. Gu (2000), Modal metasomatism in the Kaapvaal craton lithosphere: Constraints on timing and genesis from U ± Pb zircon dating of metasomatized peridotites and MARID-type xenoliths, *Contrib. Mineral. Petrol.*, *139*(6), 704–719.

Kounov, A., G. Viola, M. de Wit, and M. A. G. Andreoli (2009), Denudation along the Atlantic passive margin: New insights from apatite fission-track analysis on the western coast of South Africa, *Geol. Soc. Spec. Publ.*, *324*(1), 287–306, doi:10.1144/SP324.19.

Kounov, A., G. Viola, I. Dunkl, and H. E. Frimmel (2013), Southern African perspectives on the long-term morpho-tectonic evolution of cratonic interiors, *Tectonophysics*, *601*, 177–191, doi:10.1016/j.tecto.2013.05.009.

Kreissig, K., L. Holzer, R. Frei, I. M. Villa, J. D. Kramers, A. Kröner, C. A. Smit, and D. D. Van Reenen (2001), Geochronology of the Hout River Shear Zone and the metamorphism in the Southern Marginal Zone of the Limpopo Belt, Southern Africa, *Precambrian Res.*, *109*(1–2), 145–173, doi:10.1016/S0301-9268(01)00147-4.

Lazarov, M., A. B. Woodland, and G. P. Brey (2009), Thermal state and redox conditions of the Kaapvaal mantle: A study of xenoliths from the Finsch mine, South Africa, *Lithos*, *112*, 913–923, doi:10.1016/j.lithos.2009.03.035.

le Roex, A. P. (1986), Geochemical correlation between southern African kimberlites and South Atlantic hotspots, *Nature*, *324*(6094), 243–245.

le Roex, A. P., D. R. Bell, and P. Davis (2003), Petrogenesis of group I kimberlites from Kimberley, South Africa: Evidence from bulk-rock geochemistry, *J. Petrol.*, *44*(12), 2261–2286.

Lithgow-Bertelloni, C., and P. G. Silver (1998), Dynamic topography, plate driving forces and the African superswell, *Nature*, *395*, 345–348.

Liu, L., and M. Gurnis (2008), Simultaneous inversion of mantle properties and initial conditions using an adjoint of mantle convection, *J. Geophys. Res.*, *113*, B08405, doi:10.1029/2008JB005594.

Liu, L., S. Spasojevic, and M. Gurnis (2008), Reconstructing Farallon plate subduction beneath North America back to the Late Cretaceous., *Science*, *322*(5903), 934–938, doi:10.1126/science.1162921.

MacIntyre, R. M., and J. B. Dawson (1976), Age and significance of some South African kimberlites, in *4th European Colloquium Geochronology, Cosmochronology, Isotope Geology*, *Abstr. 66*, Amsterdam.

McMillan, I. K. (2003), Foraminiferally defined biostratigraphic episodes and sedimentation pattern of the Cretaceous drift succession (Early Barremian to Late Maastrichtian) in seven basins on the South African and southern Namibian continental margin, *S. Afr. J. Sci.*, *99*, 537–576.

Menzies, A. H., R. W. Carlson, S. B. Shirey, and J. J. Gurney (1999), Re-Os systematics of Newlands peridotite xenoliths: Implications for diamond and lithosphere formation, in *Proceedings of the 7th International Kimberlite Conference*, edited by J. M. Gurney, et al., pp. 566–583, Red Roof Design, Cape Town.

Michaut, C., C. Jaupart, and D. R. Bell (2007), Transient geotherms in Archean continental lithosphere: New constraints on thickness and heat production of the subcontinental lithospheric mantle, *J. Geophys. Res.*, *112*, B04408, doi:10.1029/2006JB004464.

Mitchell, R. H. (1995), Kimberlites, Orangeites, and Related Rocks, 410 pp., Plenum Press, N. Y.

Mitrovica, J. X., C. Beaumont, and G. T. Jarvis (1989), Tilting of continental interiors by the dynamical effects of subduction, *Tectonics*, *8*(5), 1079–1094, doi:10.1029/TC008i005p01079.

Moore, A., T. Blenkinsop, and F. (Woody) Cotterill (2008), Controls on post-Gondwana alkaline volcanism in Southern Africa, *Earth Planet. Sci. Lett.*, *268*(1–2), 151–164, doi:10.1016/j.epsl.2008.01.007.

Moore, A., T. Blenkinsop, and F. (Woody) Cotterill (2009), Southern African topography and erosion history: Plumes or plate tectonics?, *Terra Nova*, *21*(4), 310–315, doi:10.1111/j.1365-3121.2009.00887.x.

Moore, A. E., and P. A. Larkin (2001), Drainage evolution in south-central Africa since the breakup of Gondwana, *S. Afr. J. Geol.*, *104*, 47–68.

Moore, J. M., and A. E. Moore (2004), The roles of primary kimberlitic and secondary Dwyka glacial sources in the development of alluvial and marine diamond deposits in Southern Africa, *J. Afr. Earth Sci.*, *38*(2), 115–134, doi:10.1016/j.jafrearsci.2003.11.001.
Moucha, R., and A. M. Forte (2011), Changes in African topography driven by mantle convection, *Nat. Geosci.*, *4*(10), 707–712, doi:10.1038/ngeo1235.
Murray, K. E., D. A. Orme, and P. W. Reiners (2014), Effects of U-Th-rich grain boundary phases on apatite helium ages, *Chem. Geol.*, *390*, 135–151, doi:10.1016/j.chemgeo.2014.09.023.
Ni, S., E. Tan, M. Gurnis, and D. Helmberger (2002), Sharp sides to the African superplume, *Science*, *296*(5574), 1850–1852, doi:10.1126/science.1070698.
Nowell, G. M., D. G. Pearson, D. R. Bell, R. W. Carlson, C. B. Smith, P. D. Kempton, and S. R. Noble (2004), Hf isotope systematics of kimberlites and their megacrysts: New constraints on their source regions, *J. Petrol.*, *45*(8), 1583–1612.
Nyblade, A. A., and S. W. Robinson (1994), The African superswell, *Geophys. Res. Lett.*, *21*(9), 765–768.
Parsiegla, N., K. Gohl, and G. Uenzelmann-Neben (2008), The Agulhas Plateau: Structure and evolution of a large igneous province, *Geophys. J. Int.*, *174*(1), 336–350.
Partridge, T. C., and R. R. Maud (1987), Geomorphic evolution of southern Africa since the Mesozoic, *S. Afr. J. Geol.*, *90*(2), 179–208.
Pell, J., J. K. Russell, and S. Zhang (2015), Kimberlite emplacement temperatures from conodont geothermometry, *Earth Planet. Sci. Lett.*, *411*, 131–141, doi:10.1016/j.epsl.2014.12.003.
Reiners, P. W., and K. A. Farley (2001), Influence of crystal size on apatite (U-Th)/He thermochronology: An example from the Bighorn Mountains, Wyoming, *Earth Planet. Sci. Lett.*, *188*, 413–420, doi:10.1016/S0012-821X(01)00341-7.
Renne, P. R., J. M. Glen, S. C. Milner, and A. R. Duncan (1996), Age of Etendeka flood volcanism and associated intrusions in southwestern Africa, *Geology*, *24*(7), 659–662.
Ritsema, J. (1999), Complex shear wave velocity structure imaged beneath Africa and Iceland, *Science*, *286*(5446), 1925–1928, doi:10.1126/science.286.5446.1925.
Rouby, D., S. Bonnet, F. Guillocheau, K. Gallagher, C. Robin, F. Biancotto, O. Dauteuil, and J. Braun (2009), Sediment supply to the Orange sedimentary system over the last 150 My: An evaluation from sedimentation/denudation balance, *Mar. Pet. Geol.*, *26*(6), 782–794, doi:10.1016/j.marpetgeo.2008.08.004.
Rowley, D. B., A. M. Forte, R. Moucha, J. X. Mitrovica, N. A. Simmons, and S. P. Grand (2013), Dynamic topography change of the eastern United States since 3 million years ago., *Science*, *340*(6140), 1560–1563, doi:10.1126/science.1229180.
Rudnick, R. L., and A. A. Nyblade (1999), The thickness and heat production of Archean lithosphere: Constraints from xenolith thermobarometry and surface heat flow, in *Mantle Petrology: Field Observations and High Pressure Experimentation: A Tribute to Francis R. (Joe) Boyd*, edited by Y. Fei, C. M. Bertka, and B. O. Mysen, pp. 3–12, Geochem. Soc., Houston, Tex.
Rudnick, R. L., W. F. McDonough, and R. J. O'Connell (1998), Thermal structure, thickness and composition of continental lithosphere, *Chem. Geol.*, *145*(3–4), 395–411, doi:10.1016/S0009-2541(97)00151-4.
Schmitz, M. D., and S. A. Bowring (2003), Constraints on the thermal evolution of continental lithosphere from U-Pb accessory mineral thermochronometry of lower crustal xenoliths, southern Africa, *Contrib. Mineral. Petrol.*, *144*(5), 592–618, doi:10.1007/s00410-002-0419-9.
Shuster, D. L., R. M. Flowers, and K. A. Farley (2006), The influence of natural radiation damage on helium diffusion kinetics in apatite, *Earth Planet. Sci. Lett.*, *249*, 148–161, doi:10.1016/j.epsl.2006.07.028.
Skinner, E. M. W. (1989), Contrasting Group I and Group II kimberlite petrology: Towards a genetic model for kimberlites, *Kimberlites Relat. Rocks*, *1*, 528–544.
Smith, C. B. (1983), Pb, Sr and Nd isotopic evidence for sources of southern African Cretaceous kimberlites, *Nature*, *304*, 51–54.
Smith, C. B., H. L. Allsopp, J. D. Kramers, G. Hutchinson, and J. C. Roddick (1985a), Emplacement ages of Jurassic-Cretaceous South African kimberlites by the Rb-Sr method on phlogopite and whole-rock samples, *Trans. Geol. Soc. S. Afr.*, *88*, 249–266.
Smith, C. B., J. J. Gurney, N. Ebrahim, E. M. W. Skinner, and C. R. Clement (1985b), Geochemical character of southern African kimberlites: A new approach based on isotopic constraints, *Trans. Geol. Soc. S. Afr.*, *88*, 267–280.
Sparks, R. S. J., L. Baker, R. J. Brown, M. Field, J. Schumacher, G. Stripp, and A. Walters (2006), Dynamical constraints on kimberlite volcanism, *J. Volcanol. Geotherm. Res.*, *155*(1), 18–48.
Spasojevic, S., L. Liu, and M. Gurnis (2009), Adjoint models of mantle convection with seismic, plate motion, and stratigraphic constraints: North America since the Late Cretaceous, *Geochem. Geophys. Geosyst.*, *10*, Q05W02, doi:10.1029/2008GC002345.
Spiegel, C., B. Kohn, D. Belton, Z. Berner, and A. Gleadow (2009), Apatite (U-Th-Sm)/He thermochronology of rapidly cooled samples: The effect of He implantation, *Earth Planet. Sci. Lett.*, *285*(1), 105–114.
Stanley, J. R., R. M. Flowers, and D. R. Bell (2013), Kimberlite (U-Th)/He dating links surface erosion with lithospheric heating, thinning, and metasomatism in the southern African Plateau, *Geology*, *41*, 1243–1246, doi:10.1130/G34797.1.
Stevenson, I. R., and I. K. McMillan (2004), Incised valley fill stratigraphy of the Upper Cretaceous succession, proximal Orange Basin, Atlantic margin of southern Africa, *J. Geol. Soc. London*, *161*(2), 185–208, doi:10.1144/0016-764902-003.
Svensen, H., F. Corfu, S. Polteau, Ø. Hammer, and S. Planke (2012), Rapid magma emplacement in the Karoo large igneous province, *Earth Planet. Sci. Lett.*, *325*, 1–9.
Tainton, K. M., and D. McKenzie (1994), The generation of kimberlites, lamproites, and their source rocks, *J. Petrol.*, *35*(3), 787–817.
Tappe, S., D. G. Pearson, G. Nowell, T. Nielsen, P. Milstead, and K. Muehlenbachs (2011), A fresh isotopic look at Greenland kimberlites: Cratonic mantle lithosphere imprint on deep source signal, *Earth Planet. Sci. Lett.*, *305*(1), 235–248.
Tinker, J., M. de Wit, and R. Brown (2008a), Mesozoic exhumation of the southern Cape, South Africa, quantified using apatite fission track thermochronology, *Tectonophysics*, *455*(1–4), 77–93, doi:10.1016/j.tecto.2007.10.009.
Tinker, J., M. de Wit, and R. Brown (2008b), Linking source and sink: Evaluating the balance between onshore erosion and offshore sediment accumulation since Gondwana break-up, South Africa, *Tectonophysics*, *455*, 94–103, doi:10.1016/j.tecto.2007.10.009.
Torsvik, T. H., K. Burke, B. Steinberger, S. J. Webb, and L. D. Ashwal (2010), Diamonds sampled by plumes from the core-mantle boundary, *Nature*, *466*(7304), 352–355, doi:10.1038/nature09216.
van der Beek, P., M. A. Summerfield, J. Braun, R. W. Brown, and A. Fleming (2002), Modeling postbreakup landscape development and denudational history across the southeast African (Drakensberg Escarpment) margin, *J. Geophys. Res.*, *107*(B12), 2351, doi:10.1029/2001JB000744.
Zhang, N., S. Zhong, W. Leng, and Z.-X. Li (2010), A model for the evolution of the Earth's mantle structure since the Early Paleozoic, *J. Geophys. Res.*, *115*, B06401, doi:10.1029/2009JB006896.
Zhang, N., S. Zhong, and R. M. Flowers (2012), Predicting and testing continental vertical motion histories since the Paleozoic, *Earth Planet. Sci. Lett.*, *317–318*, 426–435, doi:10.1016/j.epsl.2011.10.041.